AN ABSTRACT OF THE THESIS OF

John R. Hartin for the degree of Doctor of Philosophy in Mechanical Engineering presented on May 24, 1989.

Title: Evaluation of Horizontal Axis Wind Turbine Blade Loads Using Unsteady Aerodynamics

Redacted for Privacy

Abstract approved: _____
Robert E. Wilson

Most existing analyses of the blade loads on horizontal axis wind turbines are conducted using linear steady-state aerodynamics, but evaluation of loads resulting from wind turbulence or gusts may not be adequate using these techniques. This study develops single-parameter approximations for both the shed wake and trailing wake components of the unsteady aerodynamics and incorporates them into a code that evaluates mean and cyclic blade loading. The effect on loads due to the deterministic effects of wind shear and tower interference and the stochastic effects of wind turbulence are examined. The aeroelastic equations including degrees of freedom for blade flexing and axial tower motion are solved in the time domain using turbulent wind input.

Verification of the single-parameter models is by comparison to general analytic solutions and test data available in the literature. The model for shed wake is compared to exact solutions for translating airfoils and to two-dimensional approximations for rotary-wing effects. Two

trailing wake models are evaluated using results from wind turbine tests and helicopter analysis.

Comparison of loads predictions is made to Howden 330/26 Wind Turbine data showing good agreement for cyclic and mean loads. Results show that the largest contribution from unsteady aerodynamics is an increase in mean loads due to the induced velocity lag caused by the trailing wake.

Evaluation of Horizontal Axis Wind Turbine Blade Loads Using Unsteady Aerodynamics

by

John R. Hartin

A THESIS

submitted to

Oregon State University

in partial fulfillment of
the requirements for the
degree of

Doctor of Philosophy

Completed May 24, 1989

Commencement June, 1990

APPROVED:

Redacted for Privacy

Robert E. Wilson, Professor of Mechanical Engineering

Redacted for Privacy

Gordon M. Reistad, Chairman, Mechanical Engineering Dept.

Redacted for Privacy

T. J. Maresh, Dean of Graduate School

Date thesis is presented: May 24, 1989

TABLE OF CONTENTS

LIST OF FIGURES

LIST OF TABLES

LIST OF APPENDIX FIGURES

LIST OF APPENDIX TABLES

NOMENCLATURE

Symbol	Definition
a	axial induction
$^{N}\mathbf{a}^{Q}$	acceleration of point Q in inertial frame
A	rotor area
A_0	downwash coefficient
B	number of blades
$\mathbf{b}_i$	rigid blade coordinate unit vectors
$\mathbf{c}_i, \mathbf{d}_i$	unit vectors
c	airfoil chord
C_L	lift coefficient
C_T	rotor thrust coefficient
C,F,G	Theodorsen lift deficiency functions
C',F',G'	Loewy lift deficiency functions
d	tower diameter
d_s	separation from tower to rotor plane
D	drag per unit length
e	tower velocity deficit fraction
E	material modulus of elasticity
F	Prandtl tip loss factor
F_A	blade aerodynamic load
F_r, F_r^*	generalized active and inertia forces
h	dimensionless wake distance parameter
I	area moment of inertia
k	Loewy frequency parameter
K	frequency multiplier

K_E	kinetic energy function
k_{eq}	equivalent tower stiffness
k_{ii}	stiffness matrix element
L	lift per unit length
L_0, L_1, L_2, L_W	lift components
m	apparent mass
m_{ii}	mass matrix element
M	momentum flux
M_i	moment component in $\mathbf{b}_i$ direction
n	power law exponent
$\mathbf{n}_i$	inertial frame unit vectors
$\mathbf{n}, \mathbf{r}, \mathbf{t}$	deformed blade unit vectors
$N_{\mathbf{p}}Q$	position of point Q in inertial frame
P	pressure
q	dimensionless lift parameter
q_r	generalized coordinate
Q_i	force matrix element
r	blade radial dimension
R	tip radius
$\mathbf{R}$	external force resultant
$S(r)$	deformed blade shape function
t	time
T	thrust on rotor disk
T_i	tension force component in $\mathbf{b}_i$ direction
u, u_1	axial velocity components
u_r	generalized speed
U	translating airfoil velocity

$^{N}\mathbf{v}_{r}^{Q}$	partial velocity of Q in inertial frame
V	air velocity
V_i	shear force component in $\mathbf{b}_i$ direction
V_e, V_g	potential energy functions
w	downwash
W	relative air velocity over airfoil
W_C, W_S	complex potentials for tower interference
x,y	coordinate dimensions
X	tip speed ratio, R /V
X_L	local tip speed ratio, r /V
z	blade elevation coordinate
z_0	surface roughness length
z(x,y)=x+iy	coordinates in circle plane

α	angle of attack
β	blade pitch angle
β_0	initial blade twist angle
Γ	circulation
δ	blade deflection
ϵ	slope due to blade flexing
ζ	fixed yaw angle
θ	azimuth angle
μ	blade mass per unit length
ν	blade oscillation frequency
ρ	air density
τ_s, τ_θ	time constants

ϕ	induction angle
ψ	deformed blade slope
ψ_0	rigid blade preconing angle
ω	reduced frequency
Ω	rotor rotation rate

∂	partial derivative
$(\dot{})$	time derivative
$(\,)_\infty$	freestream quantity
$(\tilde{})$	conjugate
boldface	vector quantity
1p	one cycle per revolution

EVALUATION OF HORIZONTAL AXIS WIND TURBINE BLADE LOADS USING UNSTEADY AERODYNAMICS

CHAPTER 1

INTRODUCTION

The design of Horizontal Axis Wind Turbines (HAWT) is driven by the aerodynamic loading and the dynamic response of the blades. The aerodynamic loading is a combination of the deterministic effects from wind shear, yaw, and tower interference, and stochastic effects from wind turbulence. Both are cyclic and reduce the life of the HAWT due to fatigue loading of the blades and other rotor components. Tools to accurately predict the accumulated damage caused by these loads are needed to improve the design process. The steady state performance and loads predictions for HAWT have been extensively studied, and the state of the art in loads and performance prediction is documented [1]. This thesis develops techniques and evaluates the loads that arise when unsteady aerodynamics are included. Comparisons of predictions with data form the basis for testing the accuracy of the approach.

The research was directed to develop computational methods approximating the effects of unsteady aerodynamics and to incorporate algorithms into a computer code to evaluate blade loads. A goal was to establish simple,

efficient algorithms that correctly account for the predominant physical processes but also result in a code that can be easily run on a desk-top computer in an iterative fashion for design studies. A code of this sort is admittedly a compromise between the rigor of a complex analytical formulation as presented in much of the literature and a back-of-the-envelop approach, however, the yardstick by which any model is measured is how well the results of predictions compare with data. The aim has been to develop a model that describes the rotor dynamics and aerodynamics with a first-order approximation, is tractable in that it can run in a reasonable time, yet gives agreement to data that is better than previously achieved with programs containing only steady state aerodynamics.

1.1 Rotary-Wing Aerodynamics

The basis for determination of loads on a wind turbine rotor comes from the axial momentum theory for an actuator disk developed by Rankine [2] and Froude [3] in early propeller work. Their work combined blade element theory and momentum theory into strip theory, later modified for tip loss corrections by Goldstein [4] and Prandtl [5]. A modified strip theory [6] includes wake expansion effects. Additional problems result from the fact that a considerable portion of a wind turbine blade may be stalled under certain

operating conditions, and knowledge of airfoil performance at high angles of attack is limited. Approximations that use linear aerodynamics to solve for blade loads and induction may not be adequate in such cases.

The calculation of blade loads requires a solution to both the rotor aerodynamics and the rotor dynamics. Research into the coupled rotor dynamics/aerodynamics was spurred by interest in helicopters where much of the literature on the rotary wing originated. The helicopter has many similarities with the horizontal-axis wind turbine in rotor dynamics and aerodynamics with some significant differences. The obvious difference that a helicopter rotor is producing thrust has consequences in the design of the airfoil, the structure of the wake and the interaction of the wake rotor system. The primary objective of the wind turbine rotor is to produce torque to drive a generator and the generation of thrust is a concern for the loading of the rotor and supporting structure. As a result, the design of an efficient rotor/blade system is not the same for a propulsive rotor as it is for a power generator. A helicopter in forward flight with inflow rates comparable to a windmill has the added complexity of cyclic pitch variation. A stall controlled wind turbine has fixed pitch blades, and a pitch controlled wind turbine has blades whose pitch changes at a low frequency in response to wind changes for power regulation. In addition, the induced velocity in a propeller, often termed inflow, is additive to the

velocity of air moving through the rotor disk and causes the wake to contract. In a wind turbine, the induced velocity, often termed induction, decreases the flow through the rotor causing the wake to expand. Also, a helicopter typically operates at a much higher tip speed ratio than a wind turbine rotor.

The primary difference between the rotary-wing and fixed wing unsteady aerodynamics lies in the modeling of the unsteady wakes caused by airfoil motion. Rotary wing aerodynamics present some of the most challenging problems known in computational fluid dynamics. The modeling must include not only the shed vortex wake as described in classical works by Wagner [7], Kussner [8], and von Karman [9], but must also define the helical trailing wake structure responsible for the induced velocity in the rotor plane. When a transient occurs such as a pitch change on a helicopter blade or a wind velocity change on a fixed wind turbine rotor, the fluid dynamics associated with the shed wake and the trailing wake have different response times and characteristics. There are considerable differences in the order of magnitude of the effects depending on the inflow or volume of air passing through the rotor disk as depicted in Figure 1.1.

At low inflow, the distance between the adjacent sheets of shed vorticity is small and the blade interaction with the vorticity shed by the previous blade is important. At high inflow, the spacing between adjacent sheets of shed

vorticity is large and the effects of a change in shed vorticity is small after an azimuth angle change of a fraction of a revolution. In this case the wake structure made up of the trailing vorticity results in a delay in the change in induced velocity at the rotor disk with a change in blade pitch or inflow. The effect of unsteady aerodynamics on a rotor system was first examined by Loewy [10] who extended the lift deficiency function proposed by Theodorsen [11] to a rotating harmonically oscillating blade at low inflow with a two dimensional wake approximation. At low inflow the shed wake dominates since a large trailing wake does not have time to form. Here the time constant associated with a transient is closely related to that of a fixed wing taking into account the blade interaction effects.

At high inflow, the aerodynamic state that most closely resembles the wind turbine operating conditions, the helicopter is generally in a forward flight condition and has edgewise wake distortion. In this case, the wake effects the time rate of change of the induced velocity since the wake generated by the rotor is swept downwind at a higher velocity and is not as completely influenced by the cyclic blade motion. The delay in the development of induced velocity following rapid changes in collective blade pitch were first studied by Carpenter and Fridovitch [12]. They developed an unsteady momentum model where the time constant for the change in induced velocity was based on the

apparent mass of the air accelerated through the rotor disk. These ideas were later expanded by Pitt and Peters [13] to include the effect of edge flow to become what is generally known as the dynamic inflow concept. Assumptions limiting the generality of dynamic inflow include uniform induced velocity over the rotor disk and harmonic pitch actuation, neither of which is characteristic of wind turbines.

The approximate methods developed do not have the restrictions imposed by dynamic inflow, but are instead limited by the simplifying assumptions made. There are more general computational methods that make fewer simplifications but require much more computer memory and time. Vortex theory is used to describe the rotor wake, whether for a prescribed wake of known dimension and direction, or a free wake where the wake displacement and strength are continuously calculated and updated. The wake definition in conjunction with Biot-Savart law can determine the profile of induced velocity in the rotor plane. Inviscid, potential aerodynamics are the rule in other advanced methods for dealing with rotary wing aerodynamics. Lifting surface theory [14] and lifting line theory [15] solve the linearized problem using acceleration potential method. Panel methods introduced by Hess and Smith [16] use a surface singularity such as a source, doublet or vortex to solve the linear potential equation. Formulation with this method arises from application of Green's Theorem resulting in Fredholm integral equations that must be solved on the

surface. This method has been successfully applied by a number of investigators, for example Djojodihardjo & Widnall [17] and Summa [18]. Johnson [19] has an excellent summary of the methods used including a discussion of the extension of the methods to account for compressibility and dynamic stall.

1.2 Blade Dynamics

Rotor blades are long flexible beams with in general three degrees of freedom allowing flapping motion, lag-lead motion, and torsional motion. The forces acting on the blades are the aerodynamic loads, gravitational loads, and inertial loads. The study of rotor blade dynamics was led by interest in helicopter rotor development and much of the literature in this area deals with aeroelastic studies of helicopter blades in hover or forward flight. As in the case of aerodynamics, there are many similarities and common problems that must be addressed for both helicopter blades and wind turbine rotors but it is worth noting some of the major differences between them before discussing the literature. Much of the rotor geometry is similar in that rotor/blade systems with preconing, teeter axis offset, and hingeless blades are common to both helicopters and wind turbines. The major difference is that the blades of a helicopter are very flexible and gain their strength from

the centrifugal forces generated due to high rotor speed and blade preconing, whereas wind turbines have generally stiffer blades so that the blades will not present a structural hazard when the turbine is not in operation. As a result, blade bending in any of the degrees of freedom may not be nearly as significant on the loads of a wind turbine rotor as it is on a helicopter rotor.

A general description and derivation of the governing equations of rotor dynamics are available from Johnson [20] or Bramwell [21]. The solution to the resulting equations of motion can be obtained using various numerical techniques that depend on the complexity of the equations. The sophistication of the solution is determined by the number of degrees of freedom that are retained in the equations, whether lag-lead or torsional deflections are permitted, whether intermodal coupling is included, and whether tower motion or rotation is taken into account. Retention of the nonlinear terms, including the nonlinear aerodynamics, may require a solution in the time domain. Linearized dynamics and aerodynamics can yield solutions using aeroelastic techniques. There have been numerous entries in the literature dealing with the aeroelastic problem for helicopter rotors [22-24]. Kottapalli and Friedmann [25] apply a combination of techniques to wind turbine blades by solving the nonlinear equations to obtain an equilibrium solution, then use linearized version of the equations to conduct a perturbation analysis. Similar studies examining

the aeroelastic stability of coupled wind turbine rotor/tower systems are discussed by Warmbrodt and Friedmann [26]. Recent introduction and application of the rotary-wing indicial response function for unsteady aerodynamics [27-29] have also produced very good results for both frequency domain and time domain solutions of helicopter blade loads.

The approximate solution of the coupled unsteady nonlinear rotor dynamics and aerodynamics for horizontal axis wind turbines is the topic to be presented.

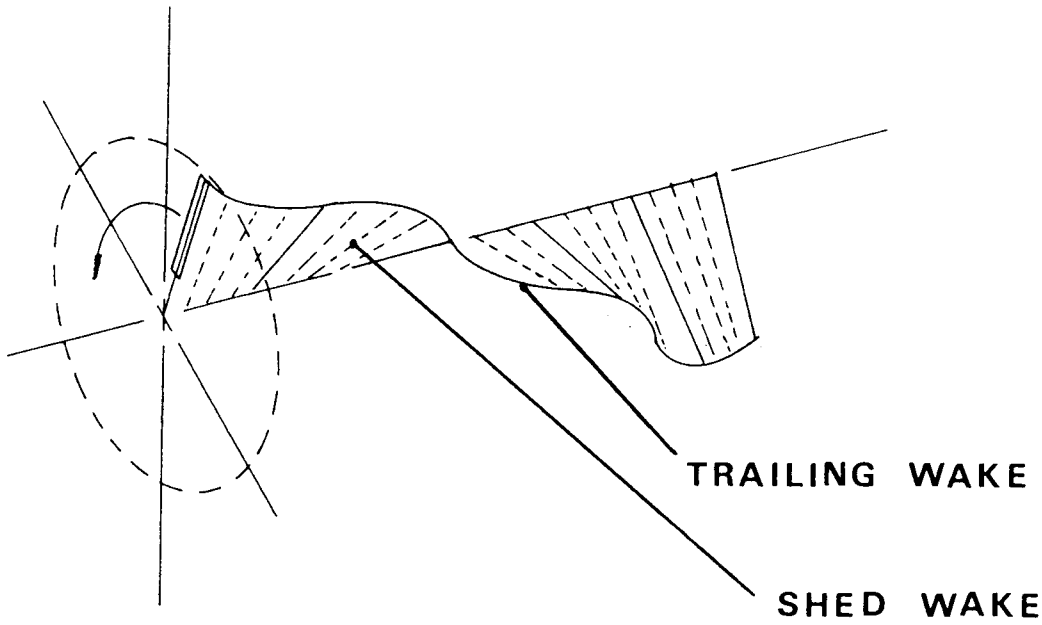

Figure 1.1 Wake Structure

1.3 References

1. Wilson, R.E., Walker, S.N., Weber, T.L. and Hartin, J.R., "A Comparison of Mean Loads and Performance Predictions with Experimental Measurements for Horizontal Axis Wind Turbines," Eighth ASME Wind Energy Symposium, Houston, Texas, Jan. 22-29, 1989.

2. Rankine, W.J.M., Transactions, Institute of Naval Architects, Vol. 6, p. 13, 1865.

3. Froude, R.E., Transactions, Institute of Naval Architects, Vol. 30, p. 390, 1889.

4. Goldstein, S., "On the Vortex Theory of Screw Propellers," Proc. Royal Soc. A123, p. 440, 1929.

5. Prandtl, L., Gottinger Nachr., p. 193, 1919.

6. Wilson, R.E. and Walker, S.N., 'Performance Analysis of Horizontal Axis Wind Turbines," NASA-NAG-3-278, 1984.

7. Wagner, H., "Uber die Entstehung des dynamischen Auftriebes von Tragflugeln," Zeitschrift fur angewandte Mathematik und Mechanik, Vol. 5, No. 1, 1925.

8. Kussner, H.G., "Zusammenfassender Bericht uber den instationaren Auftrieb von Flugeln," Luftfahrtforschung, Bd. 13, Nr. 12, pp. 410-424, 1936.

9. von Karman, T. and Sears, W., "Airfoil Theory for Non-Uniform Motion," J. Aero. Sci., Vol. 5, No. 10, 1938.

10. Loewy, R.G., "A Two Dimensional Approximation to the Unsteady Aerodynamics of Rotary Wings," Jour. Aero. Sci., Vol. 24, No, 2, 1957.

11. Theodorsen, T., "General Theory of Aerodynamic Instability and the Mechanism of Flutter," NACA TR 496, 1935.

12. Carpenter, P.J. and Fridovitch, B., "Effect of Rapid Pitch Increase on the Thrust and Induced Velocity Response of a Full Scale Helicopter," NACA TN 3044, 1953.

13. Pitt, D.M. and Peters, D.A., "Theoretical Prediction of Dynamic Inflow Derivatives," Vertica, Vol. 5, 1981.

14. Preuss, R.D., Suciu, E.O., and Morino, L., "Unsteady Potential Aerodynamics of Rotors with Applications to Horizontal Axis Windmills," AIAA J., Vol. 18, No. 4, 1980.

15. Van Holten, T., "Computation of Aerodynamic Loads on Helicopter Rotor Blades in Forward Flight Using the Method of Acceleration Potential," 9th Congress Inter. Counc. Aero. Sci., Aug. 25-30, 1974.

16. Hess, J.L. and Smith, A.M.O., "Calculation of Potential Flow About Arbitrary Bodies," Prog. Aero. Sci., Vol. 8, 1967.

17. Djojodihardjo, R.H. and Widnall, S.E., "A Numerical Method for Calculation of Nonlinear Unsteady Lifting Potential Flow Problems," AIAA J., Vol. 7, No. 10, 1969.

18. Summa, J.M., "Potential Flow about Three Dimensional Streamlined Lifting Configurations with Applications to Wings and Rotors," AFOSR-TR-74-1914, 1974.

19. Johnson, W., "Recent Developments in Rotary Wing Aerodynamic Theory," AIAA J., Vol. 24, No. 8, 1986.

20. Johnson, W., Helicopter Theory, Princeton University Press, 1983.

21. Bramwell, Helicopter Dynamics, Edward Arnold Ltd., London, 1976.

22. Ormiston, R.A. and Peters, D.A., "Hingeless Helicopter Rotor Response with Non-Uniform Inflow and Elastic Bending," J. Aircraft, Vol. 9, No. 10, 1972.

23. Piziali, R.A., "Method for Solution of the Aeroelastic Response Problem for Rotating Wings," J. Sound Vib., Vol. 4, No. 3, 1966.

24. Miller, R.H., "Methods for Rotor Aerodynamic and Dynamic Analysis," Prog. Aero. Sci., Vol. 22, 1985.

25. Kottapalli, S.B.R. and Friedmann, P.P., "Aeroelastic Stability and Response of Horizontal Axis Wind Turbine Blades," AIAA J., Vol. 17, No. 12, 1979.

26. Warmbrodt, W. and Friedmann, P.P., "Coupled Rotor/Tower Aeroelastic Analysis of Large Horizontal Axis Wind Turbines," AIAA J., Vol. 18, No. 9, 1980.

27. Venkatesan, C. and Friedmann, P.P., "New Approach to Finite-State Modeling of Unsteady Aerodynamics," AIAA J., Vol. 24, No. 12, 1986.

28. Dinyavari, M.A.H. and Friedmann, P.P., "Application of Time-Domain Aerodynamics to Rotary Wing Aeroelasticity," AIAA J., Vol. 24, No. 9, 1986.

29. Dinyavari, M.A.H. and Friedmann, P.P., "Time Domain Unsteady Incompressible Cascade Airfoil Theory for Helicopter Rotors in Hover," AIAA J., Vol. 27, No. 3, 1989.

CHAPTER 2

AERODYNAMIC MODELS

The aerodynamics of a horizontal axis wind turbine will be developed. The steady state modified strip theory will be reviewed followed by a description of the unsteady theories for shed and trailing wake. The unsteady models were developed to give a first order approximation dependent on a single-parameter. Test data and numerical results of other investigators for helicopters and wind turbines are used to verify the single-parameter algorithms. Discussion of the limitations of these methods imposed by the assumptions used and the degree of approximation is included.

2.1. Steady State Aerodynamics

The approach to be developed for the aerodynamics of a rotary-wing has its basis in the momentum theory. A simple model is developed for the axial momentum through the rotor plane which is treated idealistically as an actuator disk. Consider the streamline defined by a one-dimensional actuator disk with unrestricted flow as shown in Figure 2.1. The actuator disk is an artificial device for producing sudden discontinuities in flow properties which here represents the wind turbine rotor plane. The assumptions

included in this model are that the blades have no frictional drag, thrust loading is uniform over the disk, and no rotation is imparted to the flow. From conservation of momentum, the force per unit area on the disk can be represented for steady state flow as

$$\frac{dT}{dA} = \rho u(V_\infty - u) \tag{2.1.1}$$

From the Bernoulli equation, another expression for the force per unit area as the pressure difference across the disk

$$\frac{dT}{dA} = p^+ - p^- = \tfrac{1}{2}\rho(V_\infty^2 - u_1^2) \tag{2.1.2}$$

Solving equations 2.1.1 and 2.1.2 gives the velocity in the rotor disk as

$$u = \tfrac{1}{2}(V_\infty + u_1) \tag{2.1.3}$$

By setting $V_\infty - u = aV_\infty$, where a is defined as the axial induction, the momentum equation 2.1.1 becomes

$$\frac{dT}{dA} = 2\rho V_\infty^2 a(1-a) \tag{2.1.4}$$

Then defining the thrust coefficient for the rotor as

$$C_T = \frac{(dT/dA)}{\tfrac{1}{2}\rho V_\infty^2}$$

then, the thrust coefficient for the actuator disk operating in the windmill state can be expressed only in terms of the axial interference factor as

$$C_T = 4a(1-a) \qquad (2.1.5)$$

The effect of wake expansion in a wind turbine is an increase in thrust coefficient over that predicted by momentum theory alone. This was first addressed by Glauret who empirically [1] and analytically [2] described this effect. A comparison of Glauret's data and simple model, an MIT free wake model [3], and momentum theory is shown in Figure 2.2. A modified expression for thrust coefficient that gives a good fit to the data suggested by Wilson and Walker [4] is

$$C_T = 4aF(1-a) \qquad a < a_c \qquad (2.1.6)$$

$$C_T = C_{Tac} + \left.\frac{\partial C_T}{\partial a}\right|_{ac} (a-a_c) \qquad a > a_c$$

where the point of tangency for best fit is $a_c = 0.2$. This tangent approximation is also shown on Figure 2.2. The tip loss factor F has been given by Prandtl [5] as

$$F = \frac{2}{\pi} \cos^{-1}\{ \exp[-\frac{B(R-r)}{2r \sin\phi}] \} \qquad (2.1.7)$$

Strip theory is a combination of the axial momentum theory combined with a blade element theory, and is based on the assumption that the flow through the rotor disk can be broken into individual streamtubes that can be analyzed

independent of the adjacent flow. The streamtubes geometry used for this analysis are circular sectors defined as shown in Figure 2.3 with sides defined by radial lines $d\theta$ apart and circular arcs dr apart. Strip theory yields good results in power and load calculations where the distribution of circulation is uniform over the blade, a condition that is approximated on well designed wind turbines. The primary advantages of strip theory over vortex methods are its simplicity and reduced computational requirements. In strip theory, with each streamtube independent of the other, the calculation of induced velocity can be done sequentially rather than simultaneously.

The steady state solution of the annular stream tube element is found by setting the momentum flux in a direction normal to the blade equal to the normal force due to lift from blade element theory. The momentum flux is expressed as

$$dM = \tfrac{1}{2}\rho V_\infty^2 C_T r dr d\theta \qquad (2.1.8)$$

The normal force due to lift for the streamtube is expressed

$$dT = \tfrac{1}{2}\rho W^2 Bc C_L \cos \phi \, dr \frac{d\theta}{2\pi} \qquad (2.1.9)$$

from the velocity diagram shown in Figure 2.4. By setting

$$dM = dT$$

then

$$C_T = \frac{Bc(1-a)^2 C_L \cos\phi}{2\pi r \sin^2\phi} \qquad (2.1.10)$$

where $\phi = \tan^{-1}\left(\frac{V(1-a)}{r\Omega}\right)$ (2.1.11)

The lift coefficient C_L is a nonlinear function of the angle of attack which is found from

$$\alpha = \phi - \beta_0 \qquad (2.1.12)$$

The iterative solution of equations 2.1.6., 2.1.7., 2.1.10, 2.1.11, and 2.1.12 yield the steady state solution for thrust coefficient and induced velocity in the streamtube. This result is used to determine the magnitude and direction of lift and drag relative to the blade coordinates along the blade for the given azimuth angle step.

2.2. Unsteady Aerodynamics

Approximations for the effects of unsteady aerodynamics are formulated in terms of the strip theory. The main attributes of rotary-wing unsteady aerodynamics for a blade with fixed pitch are a lag in airfoil lift due to a shed wake and a lag in induced velocity in the rotor plane due to the trailing wake. The shed wake can be considered either as a vortex sheet or a vortex filament shed parallel to the

blade as it undergoes sudden pitch, translation, or change in velocity. The trailing wake consists of vortex filaments trailing behind and normal to the blade as shown schematically in Figure 1.1. The trailing wake is usually associated with a vortex originating only at the blade tip where the largest discontinuity in bound circulation occurs, yet actually a continuous wake is generated if circulation is not uniform along the blade.

2.2.1 Shed Wake Analysis

The effect of the shed wake on lift and moment has been described in many classical works for two dimensional, potential flow, and operational methods of treating arbitrary motion have been developed for translating and pitching wings. The operational methods are well suited to the solution of a linearized problem formulation the frequency domain where excitation can be expressed in terms of harmonic functions. An alternate approach is now developed that uses a single-parameter approximation for the circulatory unsteady lift allowing time domain solutions involving arbitrary blade motion or incident velocity. The approximate model is compared to a case where the analytical solution exists for verification.

The problem of interest here is a flapping turbine blade with time varying freestream wind that results in a

nearly constant relative velocity in the tangential direction and a variable relative velocity in the normal direction. This is analogous to an airfoil undergoing translatory oscillation. This case, shown schematically in Figure 2.5, has been solved in the literature by von Karman and Sears [6] using an analytical approach that gives a closed form expression since the wake integrals result in defined functions. The same problem has been solved using a numerical approach based on vortex method by Wilson, et. al. [7]. This vortex method, using the simplifying assumptions that the shed vorticity remains along the blade axis and does not curl up, calculates the net circulation strength about the airfoil by tracking the position and strength of the shed vortices. As each vortex is shed, the net circulation about the airfoil is updated and the lift is calculated. This method becomes limiting since each time step adds two new vortices, a shed vortex and and image vortex, and the computational time increases with each increase in the number of vortices. The vortex method compares very well with the von Karman and Sears solution at a selected frequency as shown in Figure 2.6. The results shown here represent approximately 130 vortices in the system.

The assumptions inherent in the analytical development used by von Karman and Sears are that the fluid is incompressible and inviscid, the flow is two-dimensional, and the oscillations and thickness are small compared to the

chord. An airfoil undergoing translatory oscillations sees a uniform downwash over the chord given by

$$w = A_0 U e^{i\nu t} \tag{2.2.1}$$

where the frequency is defined in terms of a multiple of the airfoil translating velocity U divided by the airfoil chord as $\nu = KU/c$.

The lift is the sum of three components

$$L = L_0 + L_1 + L_2 \tag{2.2.2}$$

where L_0 is the quasi-steady lift, L_1 is the non-circulatory lift due to the apparent mass, and L_2 is the component of lift due to the wake effect. The quasi-steady term is given by

$$L_0 = \rho U \Gamma \tag{2.2.3}$$

and the circulation can be expressed in terms of the downwash as

$$\Gamma = \pi c w \tag{2.2.4}$$

$$\text{then} \quad L_0 = \pi A_0 \rho c U^2 e^{i\nu t} \tag{2.2.5}$$

The added mass term is determined by multiplying the apparent mass of a flat plate ($\rho\pi c^2/4$) times the acceleration of the airfoil (dw/dt) to give

$$L_1 = i\left(\frac{\pi}{4}\right) A_0 K \rho U^2 c e^{i\nu t} \tag{2.2.6}$$

The wake term for this case can be expressed in terms of modified Bessel functions or more concisely in terms of Theodoreson's [8] lift deficiency function $C(\omega)$ as

$$L_2 = -L_0(1 - C(\omega)) \tag{2.2.7}$$

where the reduced frequency defined by $\omega = \nu c/2U$
Noting that $\omega = K/2$, and defining a dimensionless lift parameter q as

$$q = \frac{L}{\rho U^2 c} \tag{2.2.8}$$

then the total dimensionless lift can be given by

$$q = \pi A_0 \left(C\left(\frac{K}{2}\right) + i\frac{K}{4} \right) e^{iKUt/c} \tag{2.2.9}$$

The single-parameter solution is formulated in a somewhat heuristic manner. The circulatory quasi-steady lift and wake effect are lumped together into what has been called in literature a augmented state variable that is defined by a first order differential equation characterized by a single-parameter time constant. Establishing that the initial and final values must agree with the characteristics of the classical Wagner function dictates the form of equation. These conditions are

$L_{circ}/L = \frac{1}{2}$ at $t=0$

$L_{circ}/L = 1$ at $t=\infty$

Letting $L_{circ} = \frac{1}{2}L_0 + \frac{1}{2}L_W$, then the augmented state equation defining L_W is

$$\tau_s \frac{dL_W}{dt} + L_W = L_0 \qquad (2.2.10)$$

where τ_s is the shed time constant. Noting that $q_{circ} = L_{circ}/\rho U^2 c$, then the solution of the augmented state equation is

$$q_{circ} = \tfrac{1}{2}\left(1 + \frac{1}{1+\nu\tau_s}\right) e^{i\nu t} \qquad (2.2.11)$$

It is important to note that the result given in this form assumes that the quasi-steady lift term L_0 is a simple harmonic function of the form given in equation 2.2.5. This is used now for the purpose of generating a result that can be compared to the other methods. In practice, when equation 2.2.11 is solved numerically for an arbitrary quasi-steady lift, there are no restrictions on its form. Adding the non-circulatory apparent mass term L_1 gives

$$q = \frac{\pi A_0}{1+\nu^2\tau_s^2}\left\{\left[1+\tfrac{1}{2}\nu^2\tau_s^2\right] + i\left[\tfrac{1}{4}K(1+\nu^2\tau_s^2) - \tfrac{1}{2}\nu\tau_s\right]\right\}e^{i\nu t} \qquad (2.2.12)$$

A comparison of the single-parameter result with the exact solution at $\nu = 2U/c$ is shown in Figure 2.7, showing an agreement as good as the vortex method at this frequency.

An evaluation of the single-parameter method over a range of possible frequencies is made by comparing the magnitude and phase of the dimensionless lift function $q/\pi A_0$ in the form of frequency response plots as shown in Figure 2.8. The frequency is given in terms of the dimensionless multiplier K. The time constant that provides the best fit of the single-parameter method to the exact solution over the range of frequencies is $U\tau_s/c = 2.5$ as shown. This approximation agrees very well at the high and low frequency limits, but has as much as ten percent error in magnitude and ten degrees in phase between the frequencies of 0.1 U/c and 1.0 U/c.

The single-parameter approximation is easily solved numerically for an arbitrary downwash as experienced by a wind turbine. The apparent mass component, although generally small in air, is readily determined from the blade kinematics. The frequency range of interest for a wind turbine blade is determined by considering the energy content of the rotational wind turbulence spectrum. Data taken from the Howden machine, which is used for comparison of loads data in Chapter 4, indicates that most of the wind energy from turbulence experience by the blade occurs at multiples of rotational frequency. The first peak occurs at a frequency equal to the blade rotational frequency and is driven primarily by the wind shear. At this frequency, using $U = r\Omega$ for the rotating blade, the frequency parameter becomes $K = c/r$. The next largest peak occurs at

twice the rotational frequency giving K = 2c/r. For the Howden machine, the peak at 2Ω is large since this frequency of 1.4 Hz is very close to the blade flapping natural frequency of 1.43 Hz. Above this frequency, the wind power spectral density decreases. The range of K where it is important for the shed wake model to be valid then lies within $c/r < K < 2c/r$, $0 < r < R$. For the blade geometry defined in Appendix A, the chord to radius ratio ranges from c/r = 1.6 at the hub to c/r = 0.06 at the blade tip making $0.06 < K < 3.2$. Referring to Figures 2.8(a) and 2.8(b), the model is valid and shows good agreement with the exact solution in this range.

The von Karman and Sears solution, vortex solution, and approximate solution were all generated considering translating airfoils. Not resolved is the question of the magnitude of the effect of the rotational wake on the nature of the solution or the value of the time constant. The original work on unsteady rotary wing aerodynamics was done by Loewy [9] when he generated a two dimensional wake model for a low inflow rotor with an airfoil undergoing pitch oscillations. The result of his work is a modified lift deficiency function C'(k) that is a function of the frequency ratio ν/Ω and the distance between successive rows of vorticity measured in half-chords, $h = 4\pi V_\infty/cB\Omega$. Loewy's results for a non-oscillating blade are reproduced here, showing F'(k) and G'(k) in Figure 2.9, where C'(k) = F'(k) + iG'(k), and noting that Loewy's k = K/2. As h approaches

infinity, Loewy's lift deficiency function approaches Theodoreson's result for a translating airfoil. For h>5, the error between the two is small and the results of the translating airfoil will be applicable to the rotating wing. The question then becomes under what operating conditions for a wind turbine is the distance h large making the rotary wake effect negligible.

There are two operating regimes for a typical wind turbine for which the distance h is large and the approximation method discussed is justified in ignoring the rotary wake. At high wind speeds, where the loads approach the design loads, the inflow is very high and the induced velocity is small causing h to become very high. Also, during startup and shutdown, when loads are again high, the rotor rotation rate is low and again h is very large. The operating condition for which h is small and the approximation is not good is at low wind speeds when inflow is low and the induced velocity is high. Although this affects the accuracy of the one parameter approximation, the justification is that for the conditions that the model incorrectly ignores the previous shed wake, the energy capture and loads are small and are not the design drivers. As an example, the Howden machine has values of h = 4 for the cut-in wind speed of 6 m/s and a value of h = 20 at the cut-out speed of 28 m/s. For h near 4, neglecting the previously shed wake introduces some error.

It is worthwhile to note that the problem has been approached by other investigators and good approximations have been obtained that include the rotary wake by developing a second order equation. This results in a set of two first order simultaneous equations defining augmented state variables. The disadvantage of the method presented is that the state variables are arrived at empirically and vary depending on the configuration. The single-parameter method, although tailored by comparison to theory, has a fixed time constant. The second order method has been applied to the time domain solution of aeroelastic problems in helicopter hover and forward flight [10,11] with good results.

2.2.2 Trailing Wake Analysis

While the effect of the lift lag due to shed wake is to cause a reduction in loads, the lag in the change in induced velocity due to the trailing wake causes a considerable increase in blade loads since the magnitude of the relative wind normal to the blade is the difference between the free-stream and induced velocities. This means that if the induced velocity lags, the load initially reacts to the larger change in free-steam velocity. Two different approaches have been examined to analyze the effect of the trailing wake on the induced velocity in the rotor plane. The goal was to develop a first order model of the lag

effect without tracking the trailing vortices in the wake requiring extensive calculations.

2.2.2.1 Convective Model

The convective model was developed along the lines of the method originated by Montgomerie [12] and consists of using a simple ring model of the turbine wake and determining an induced velocity time constant from analysis of the shed rings being convected in the wake.

Consider the helical wake structure of the steady state wake of a wind turbine rotor or propeller as depicted in Figure 2.10. According to Helmholtz' rule, the vorticity is a continuous structure consisting of a section of bound vorticity on the blade, shed vorticity parallel to the blade, a center-line component that contributes to wake rotation, and the helical trailing wake, neglecting the effect of wake expansion discussed in section 2.1. Although the vorticity is shed with varying strength along the length of the blade due to non-uniform circulation, only the tip vortex is shown. The Biot-Savart law yields the induced velocity at any point (x,y,z)

$$\mathbf{V}(x,y,z) = \frac{\Gamma}{4\pi} \int \frac{(\mathbf{r} \times d\mathbf{R})}{r^3} \qquad (2.2.13)$$

The effect of a sudden change in wind velocity approaching the rotor is a change in the pitch of the helix trailing

from the airfoil. The induced velocity at the rotor plane changes as the pitch change is convected into the wake and a new equilibrium is established. The instantaneous axial velocity component of the induced velocity at any point in the rotor plane is found by integrating equation 2.2.13 along the deformed helix, a process that is computationally burdensome. The calculation time can be improved somewhat by using a method proposed by Graber and Rosen [13] that places bounds on the integration. That is, the functions describing the envelop of the near and far wake can be integrated analytically giving bounding the solution and shortening the number of calculations to convergence. Even with more efficient algorithms, calculating the induced velocity at each blade an azimuth angle increment by integration along the wake is prohibitive for a code to be used on desk-top computers.

An approximation proposed by Montgomerie uses a simpler wake model composed of a sequence of vortex rings instead of the helix as shown in Figure 2.11. Then, when a sudden change in wind velocity occurs, a rings with a new vortex strength ar propagated through the wake. The calculations are further simplified by considering only the magnitude of the axial induced velocity along the x-axis. Then for a single ring as shown in Figure 2.12, the axial induced velocity, expressed in terms of the induction **a** , is given by the closed form expression

$$a_i = \frac{V_i}{V} = \frac{\Gamma_i}{2RV} \left[1 + (x_i/R)^2\right]^{-3/2} \qquad (2.2.14)$$

Then, for a sequence of rings,

$$a = \sum_{i=1}^{n} a_i \qquad (2.2.15)$$

The velocity at which the vortex rings a swept downstream can be estimated from principles developed from the momentum theory. The average velocity in the wake is bounded by the velocity at the rotor plane $u = V_\infty(1-a)$ and the velocity far downwind $u = V_\infty(1-2a)$. Averaging these, Montgomerie used $u = V_\infty(1-1.5a)$. A more accurate result can be achieved by using the Biot-Savart law with a helical wake. Integration give the actual velocity at any position in the wake as

$$u = V_\infty \left\{1 - a \frac{x/R}{\left[1+(x/R)^2\right]^{\frac{1}{2}}}\right\} \qquad (2.2.16)$$

The choice of the velocity at which the vortex rings are swept downwind in the wake influences the time constant for induced velocity lag, especially when the initial value of induction is high. Other than those chóices discussed, some argument could also be made for using either the free stream velocity or the far downwind velocity, or some weighted average. A comparison of the effect of this choice is presented in Figure 2.14 for a three blade rotor. The time constant increases as the ring velocity is reduced, as the

initial value of induction is increased, and as the tip speed ratio is increased. This indicates that the section of blade near the tip that has a higher local tip speed ratio and loading will have a longer time constant than the inner portion of the wake. It is interesting to note also that the weighted wake velocity obtained using equation 2.2.16 is very near the velocity of the far wake and not the average velocity suggested by Montgomerie.

There is also some sensitivity of the time constant to the location of the position of the first ring. Montgomerie placed the first ring, after $2\pi/B$ radians of rotor revolution, at a distance $d(x/r) = Vdt = V\ (2\pi/B\Omega)$, but some argument can be made for placing the first ring at some fraction of that distance. It turns out that the placement of the initial ring become significant only when the number of rings required for equilibrium is small (<10) which occurs at tip speed ratios less than 1. For many wind turbines, the tip speed ratio at the blade tip is typically in the range of 5 to 10, so a tip speed ratio of 1 is for the lower 20% or less of the blade where loads are not significant.

The procedure is to start at some initial value of induced velocity a(0) and follow the change in induction as rings are added and convected downwind into the wake. As each new ring is added, all the existing rings move a distance

$$dx = udt = u \frac{2\pi}{X_L B} \tag{2.2.17}$$

A new equilibrium induced velocity is reached when the addition of a new ring no longer causes a change in the induced velocity at the rotor plane. What is of interest is not the new equilibrium level, but how many rings were generated before the change with each new ring was within some convergence criteria. Montgomerie recognized that the characteristic of the change in induced velocity was approximated exponential in form, and proposed that the process could be modeled with a first order equation of the form

$$\tau_\theta \frac{da}{d\theta} + a = a_{QS} \tag{2.2.18}$$

where a_{QS} is the quasi-steady axial induction found from the steady state momentum theory. The time constant is found by determining the change in induction as a function of a(0), X_L, B, and the number of rings, and estimating the number of rings when $a/a_{QS} = e^{-1}$. The value of these time constants, expressed in terms of rotor azimuth angle instead of number of rings, is shown in a graphical form for a three-blade rotor in Figure 2.14. Some error in estimating the value of the time constant is introduced by modeling the growth in induction as an exponential function since the curve of growth in induction is only approximately exponential.

2.2.2.2 Unsteady Momentum Model

The unsteady momentum model treats the delay in the change of induced velocity at the rotor without directly dealing with the wake characteristics, thus avoiding the computational problem of tracking vorticity in the wake. This theory is instead an extension of the steady-state momentum theory developed in section 2.1 which buries the wake characteristics in the semi-empirical thrust coefficient term. The model was originally proposed by Carpenter and Fridovitch [14] for analysis of loads on hinged helicopter blades. Since then, the idea has been developed for helicopter analysis under the name of dynamic inflow. In dynamic inflow, even though results in the literature have shown impressive correlation [15] and provided good results for helicopters in hover, there is no general theory to predict time constants. The difficulty arises form the coupled rotor/inflow, where loads calculations, blade dynamics, and induced velocity are interdependent. Also, the limitation imposed on the helicopter work, that the inflow or induced velocity is uniform over the rotor disk, is restrictive and not necessarily valid for a heavily loaded rotor. A more general first order formulation using axial flow and flap-wise dynamics using the strip theory assumptions will be presented.

The basis of the theory lies in an application of Newton's Second Law to the air mass passing through the actuator disk. That is, a difference between the blade element thrust and the force from momentum flux due to an non-equilibrium induced velocity causes either an acceleration or deceleration of an air mass through the rotor until a new equilibrium is established. This imbalance, given in terms of the blade element expressions already derived is

$$dT - dM = dm \frac{du}{dt} \tag{2.2.19}$$

where the blade element force dT is from equation 2.1.8 and the momentum flux is from equation 2.1.9. The elemental air mass accelerated by the unbalanced forces is typically taken to be the virtual mass of an impermeable circular disk given by Batchellor [16]. The differential mass expressed in terms of radius is

$$dm = 8\rho R[1-(r/R)^2]^{\frac{1}{2}} r dr \frac{d\theta}{2\pi} \tag{2.2.20}$$

The integral of dm over the rotor disk yields a total virtual mass of $8/3\,\rho\,R^3$. The potential flow assumptions used in the derivation of this value give an unrealistic flow condition of infinite velocity at the disk edge, and the impermeability of a two or three blade rotor is easily questioned.

The resulting nonlinear first order equation describes the lag in induction in the same manner as the approximate first order equation generated using the convective model. Substituting $u/V_\infty = a$ and $V_\infty t/R = \theta/X$, the equation can be expressed in terms of the induction and the azimuth angle as

$$\frac{da}{d\theta} = \frac{(Bc/R)C_L\,[(V_n/V_\infty - a)^2 + X_L^2]^{\frac{1}{2}} - 2\pi C_T/X}{16\,[1 - (r/R)^2]^{\frac{1}{2}}} - \frac{a\,dV_\infty}{V_\infty\,d\theta} \qquad (2.2.21)$$

Note that V_n is the relative wind velocity normal to the rotor plane. The time domain solution (in terms of azimuth angle instead of actual time) is then easily carried out without the iteration on induced velocity required for the steady state and convective solutions. The only approximations inherent in this method are those normally associated with strip theory and those concerned with the apparent mass.

Table 2.1 compares the basis and limitations of the two different models for trailing wake effects. The convective model is derived from a simple wake model while the unsteady momentum model is not wake dependent except empirically in the determination of the thrust coefficient from strip theory.

2.3. Model Verification

The ideal case for model verification would come from a fully instrumented, well controlled test of a rotor with simple geometry and documented physical properties. Such data for wind turbines undergoing transients is not readily available.

One test case comes from some preliminary test results recently presented for transient load and power on a wind turbine whose blades are given step changes in pitch [17]. The Danish wind turbine Nibe B is a three blade, 630 KW machine with full span pitch of its cantilevered blades. The tests were conducted with a relatively constant wind speed of 8 to 9 meters per second, and the blades were pitched at approximately 1.5 degrees at frequencies of 0.014 Hz to 1.5 Hz. The results for the time history of bending moment and power give a time constant of approximately 9 seconds, which is equivalent to 5 revolutions. At the test conditions, the local tip speed ratio at the tip is $X_L = 8$, and the value of axial induction is a = 0.3 to 0.4. Using these estimates, the convective method would predict a time constant of 2.1 to 3.2 revolutions based on Figure 2.14, about half of the test results. The unsteady momentum method would be expected to yield a somewhat shorter delay based on the discussion of the previous section.

Comparison of the delay predicted by the two methods can be done readily if some simplifying assumptions are made. Ignoring the tip correction and assuming linear aerodynamics with $C_L = 2\pi\sin\alpha$ and a fixed pitch $\beta_0 = 0$, then the steady state induction found from equations 2.1.8 and 2.1.9 is uniform and given by

$$a_{STEADY} = \tfrac{1}{4}(Bc/R)X \qquad (2.3.1)$$

The convective method then gives the induction as

$$\frac{da}{d\theta} = \frac{a_{STEADY} - a}{\tau_\theta} \qquad (2.3.2)$$

where τ_θ is the time constant found from Figure 2.14 expressed in azimuth angle. Similarly, making the same assumption for uniform induction, the unsteady momentum induction equation 2.2.19 can be expressed as

$$\frac{da}{d\theta} = \frac{3\pi}{16}(Bc/R - 4a/X)(1-a) \qquad (2.3.3)$$

These simplified equations are solved numerically for given initial conditions to give the time history of induction for a step change in steady state conditions. Using representative values of $Bc/R = 0.3$ and $X = 5$, the results are given in Figure 2.15. The unsteady momentum method predicts a shorter delay than the convective method conflicting with the data from the Nibe B test which

measured the induction time constant to be longer than the convective prediction.

Another test case for the theories discussed comes from some testing and numerical modeling of a sub-scale helicopter rotor. Some aspects of the model are not included since no simplified models for wake contraction for a propulsive rotor exist in the same form as the tangent model employed for the expanding wind turbine wake. Otherwise, the models for shed wake and trailing wake are adaptable to analysis of a hovering helicopter.

The sub-scale rotor used for wake studies by Gray and Brown [18] was the same configuration used by Summa [19] for numerical studies of impulsive starts. The rotor characteristics are:

Number of blades: 1 - Gray and Brown [18]
1 and 4 - Summa [19]

Tip Radius R = 1.22 m

Hub Radius r_H = 0.22 R

Chord c = 0.1524 m

Collective Blade Pitch: Variable - Gray and Brown [18]
Fixed (13.75 degrees) - Summa [19]

Airfoil: NACA 0015 - Gray and Brown [18]
Flat Plate - Summa [19]

Steady state test results of a one blade rotor in hover ($X = \infty$), given in the form of thrust coefficient as a function of blade collective pitch angle are shown in Figure 2.16 compared to the predicted thrust coefficient based on

steady state strip theory. The strip theory prediction, which does not include effects of wake contraction agrees very well except at higher blade loading where contraction effects become more significant.

An evaluation of the unsteady aerodynamic models comes from numerical predictions of the same rotor undergoing an impulsive start. These predictions by Summa were generated using a Green's function approach to the solution of three dimensional lifting potential flows where the velocity potential at any point in the fluid is represented by a distribution of doublets. Summa's model includes features for the roll-up of the starting vortex and modeling of the distorted rotor wake geometry. The process of calculating the geometry of an unconstrained wake involves shedding the vortices at the trailing edge then determining the displacement of each shed element with time based on a calculation of the velocity distribution in the flowfield. Each azimuth angle increment increases the size of the set of simultaneous equations that must be solved to determine the circulation and lift on the blade sections. The results presented by Summa are for a limited number of panels, (10), and a limited azimuth angle range of 300 degrees for the case of inflow equal to 0.05 and 120 degrees for the other cases. Summa's goal of converging to the exact solution limits the practicality of his methods.

Application of the approximate solution to his problem require some reformulation of the shed wake problem to

examine the growth in circulation from zero (Kussner problem) rather than a change in circulation from a quasi-steady value (Wagner problem). Also, since Summa assumed a rigid rotor, there is no requirement for an added mass term due to blade motion. As a result, since L_0 and L_1 are zero, the wake term becomes the only circulatory lift term, i.e.

$$L_{circ} = L_W \tag{2.3.4}$$

where,

$$\tau \frac{dL_W}{d\theta} + L_W = L_{STEADY} \tag{2.3.5}$$

with L_{STEADY} being the asymptotic value of lift for the non-oscillating blade. The initial condition is $L_W(0) = 0$.

The convective and unsteady momentum models were used to generate predictions of rotor thrust for an impulsively started rotor of the same configuration employed by Summa and Gray and Brown. The convective model changes only due to the sign change in induced velocity so that the velocity that the wake is convected downwind is increased. This results in a new family of curves for the time constant depending on the number of blades, tip speed ratio, and initial induction. For the momentum model of a propulsive rotor in hover, V_n is constant, $V_n/V_\infty = 1$, the sign on induced velocity changes, and the thrust coefficient is evaluated from momentum theory (equation 2.1.5). This model gives the equation

$$\frac{da}{d\theta} = \frac{(Bc/R)C_L\,[(1+a)^2 + X_L^2]^{\frac{1}{2}} - 8\pi aF(1+a)/X}{16\,[1 - (r/R)^2]^{\frac{1}{2}}} \qquad (2.3.6)$$

For an impulsive start, the rotor is assumed to have no initial lift or induction. Comparisons between the methods indicates that the convective method predicts as much as a fifty percent longer delay time for the impulsive start which is consistent with the predictions for wind turbines. The difference that would be seen between the methods for sinusoidal inputs more typical of the velocity input to a turbine or helicopter depends on the frequency range of the signal. A comparison between Summa's vortex methods and the approximate methods is shown in terms of the thrust coefficient per blade for a four-blade rotor as a function of azimuth angle in Figure 2.17 for three cases of inflow corresponding to X = 20, X = 57, and X = ∞. These results show a very good agreement both qualitative and quantitative between the vortex method and the approximate formulation for an impulsive start, with the approximate methods requiring a small fraction of the computation time of the vortex method.

Table 2.1 Trailing Wake Model Comparison

	CONVECTIVE	UNSTEADY MOMENTUM
Reference	Montgomerie [12]	Carpenter & Fridovitch [14]
Physical Model	Ring Vortex Wake Model	Force Balance on Rotor Disk
Mathematical Form	First-Order, Linear (2.2.18)	First-Order, Nonlinear (2.2.21)
Controlling Parameter	Wake Time Constant Determined from Assumed Wake Velocity	Apparent Mass Distribution Based on Impermeable Disk
Approximations & Assumptions	1) No Wake Expansion 2) Only Axial Induction on Centerline Used 3) Exponential Form is Approximate	1) Strip Theory Limitations with Non-Uniform Induction 2) Neglects Rotational Induction

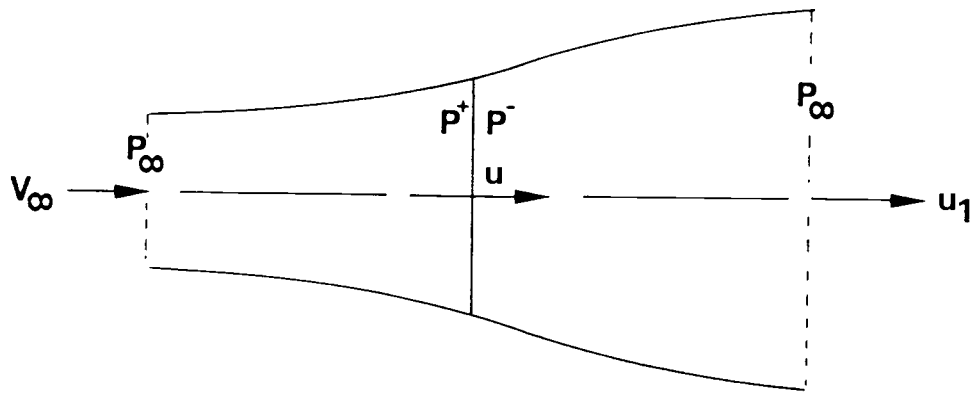

Figure 2.1 Actuator Disk Flow Model

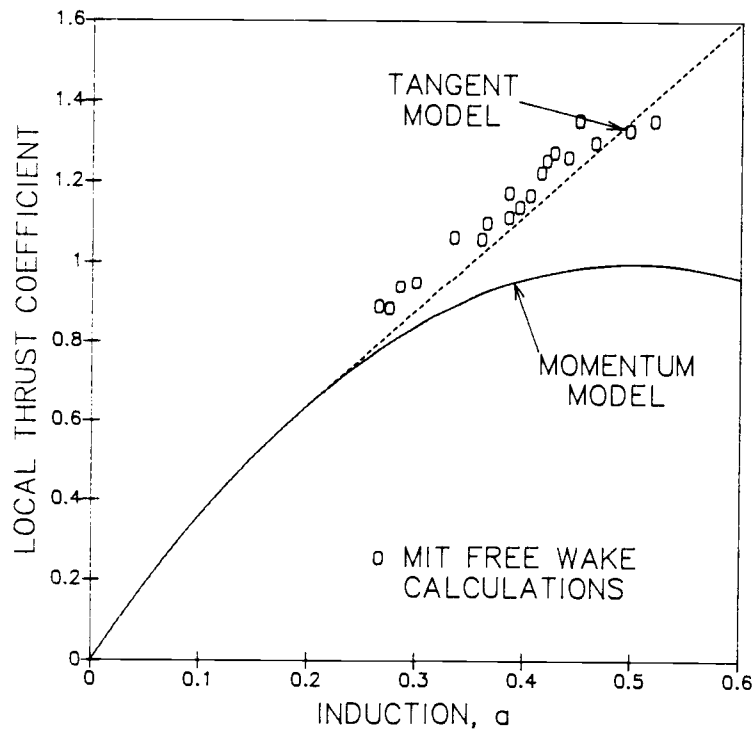

Figure 2.2 Ideal Thrust Coefficient vs. Axial Induction

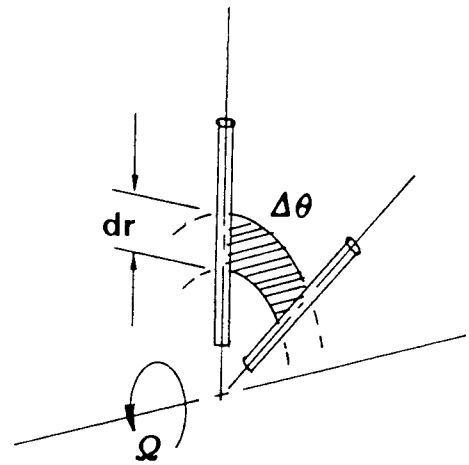

Figure 2.3 Streamtube Element

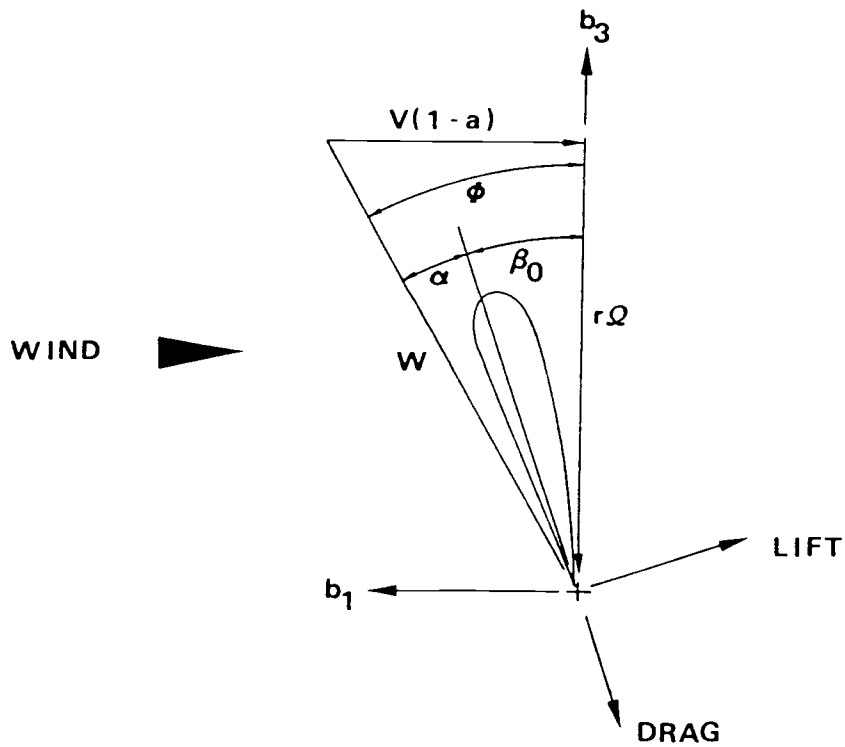

Figure 2.4 Airfoil Velocity Diagram

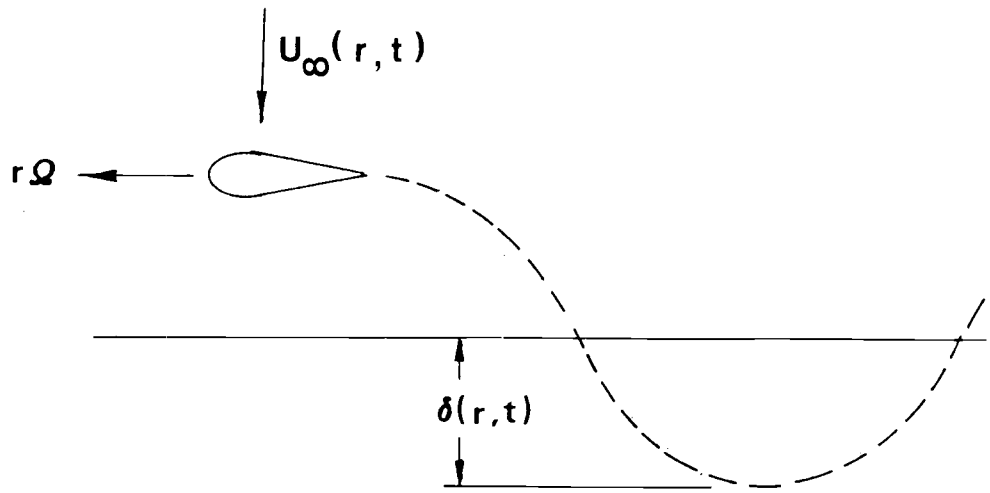

Figure 2.5 Flapping Blade with Variable Freestream

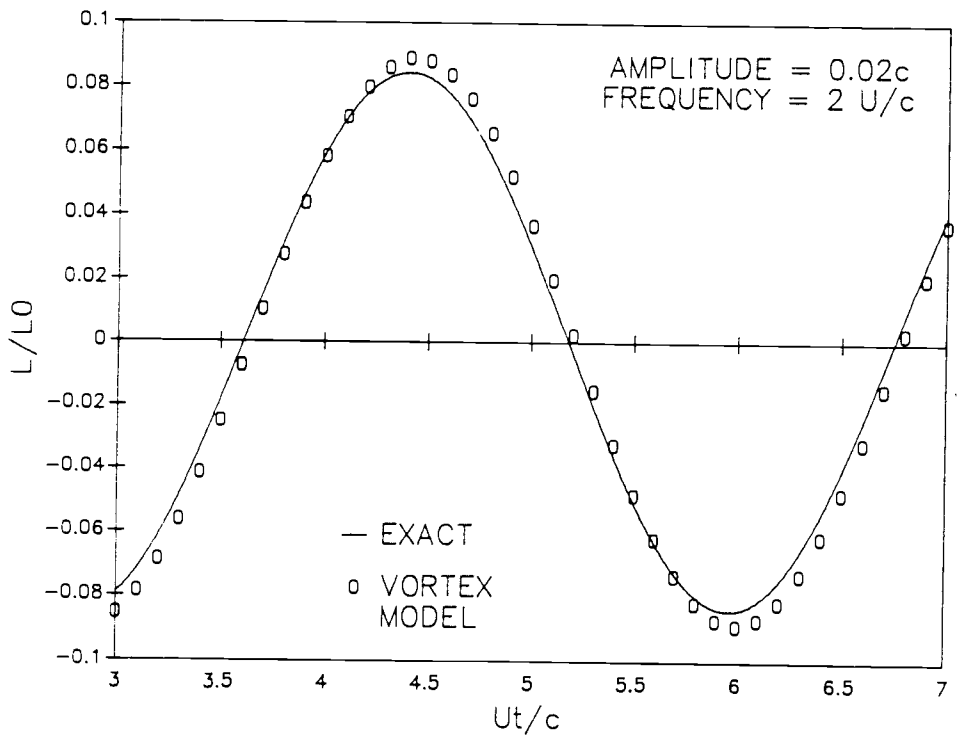

Figure 2.6 Comparison of von Karman-Sears Solution with Point Vortex Method

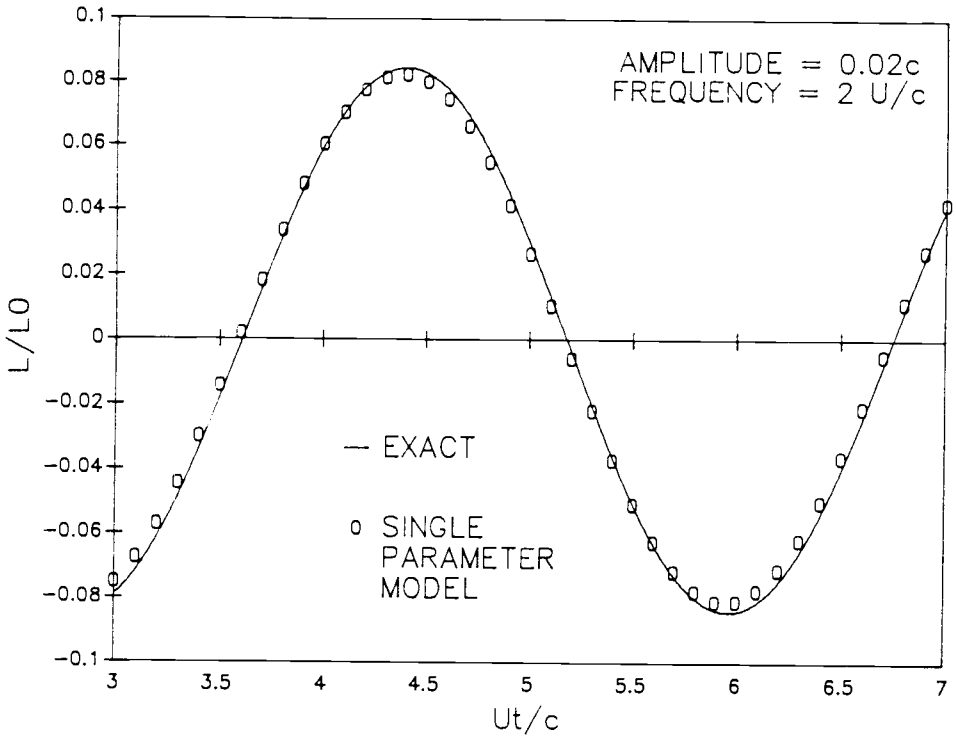

Figure 2.7 Comparison of von Karman-Sears Solution with Single Parameter Method

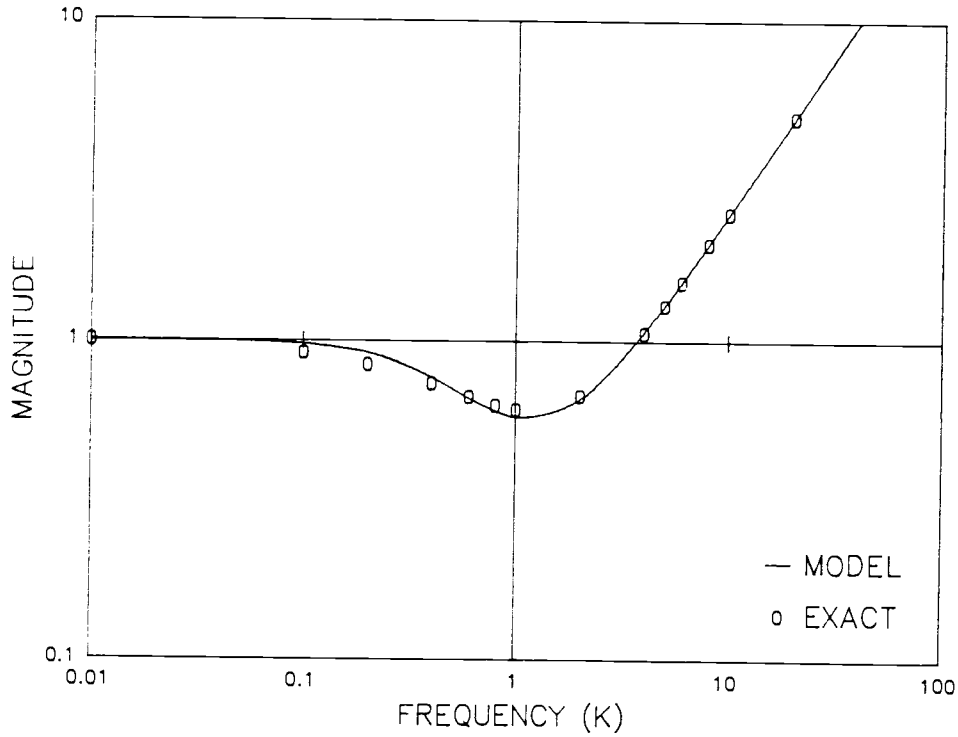

Figure 2.8(a) Magnitude Comparison of Exact Solution with Single Parameter Model

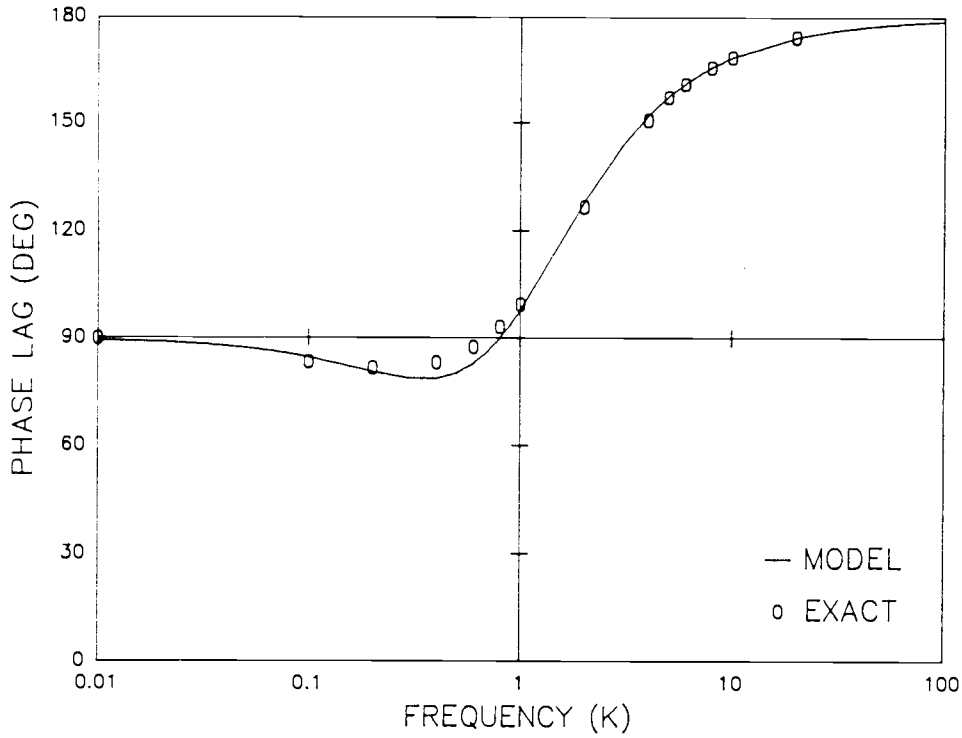

Figure 2.8(b) Phase Comparison of Exact Solution with Single Parameter Model

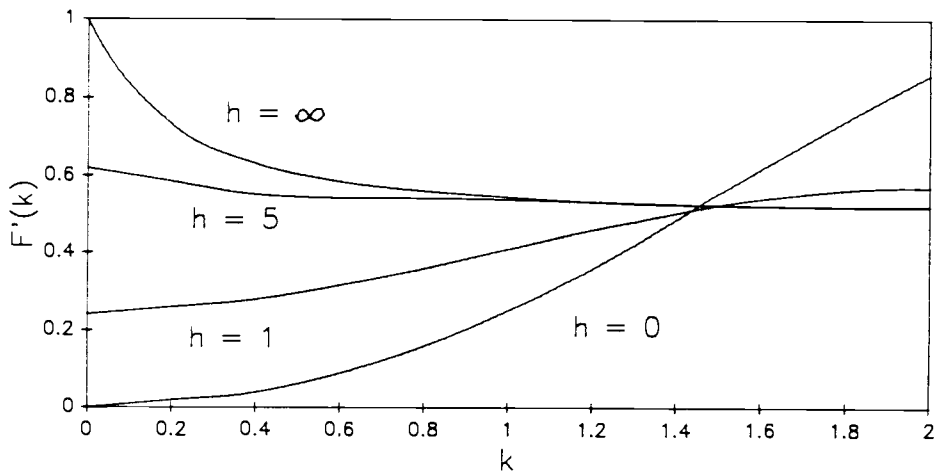

Figure 2.9(a) Loewy's F' vs. k as a Function of Inflow Parameter h

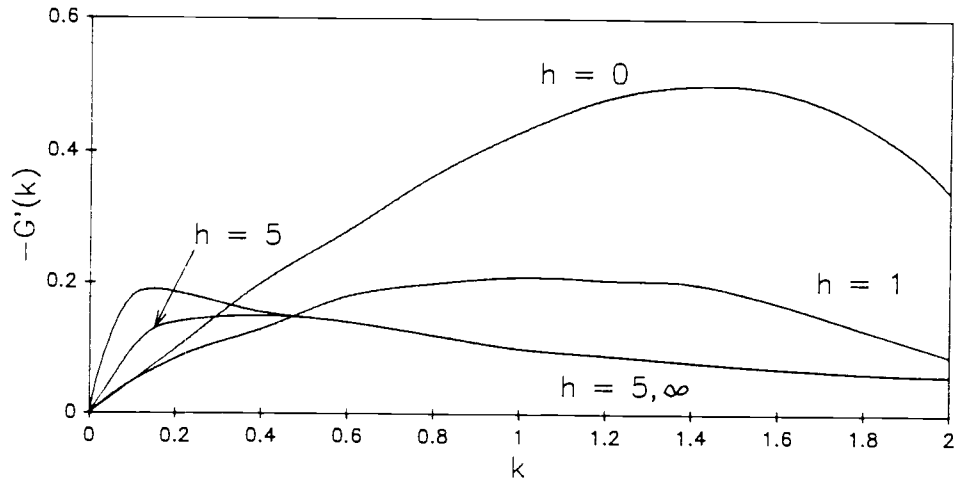

Figure 2.9(b) Loewy's -G' vs. k as a Function of Inflow Parameter h

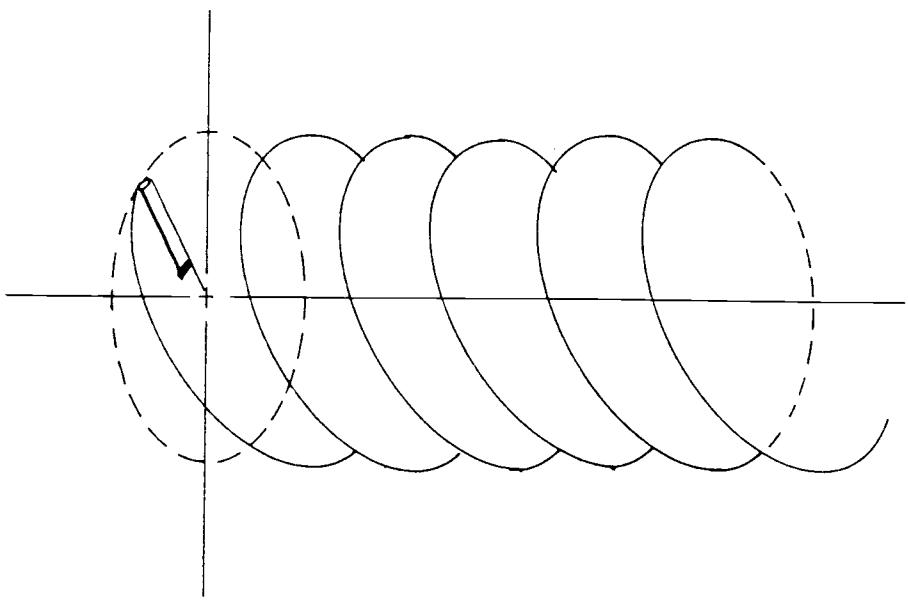

Figure 2.10 Rotor Helical Wake Model

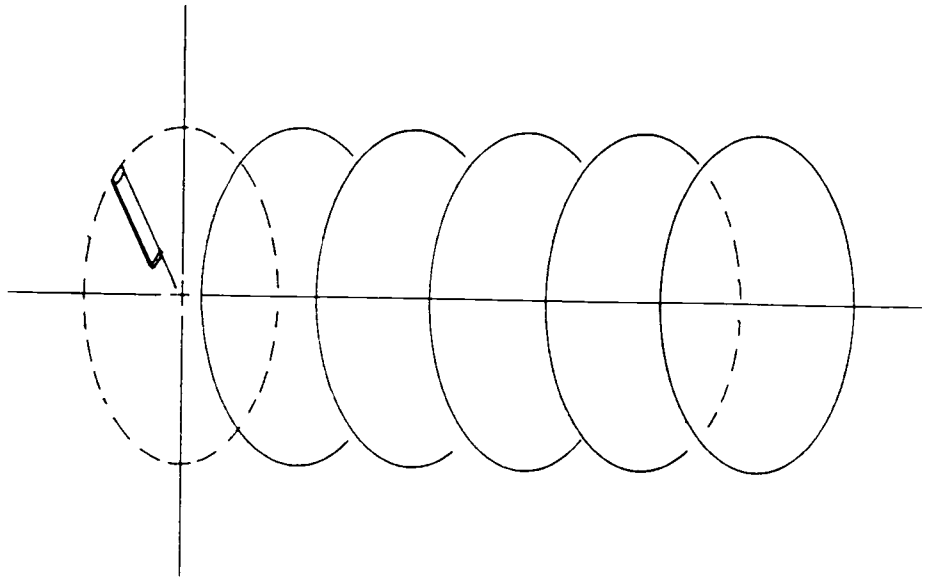

Figure 2.11 Rotor Ring Vortex Model

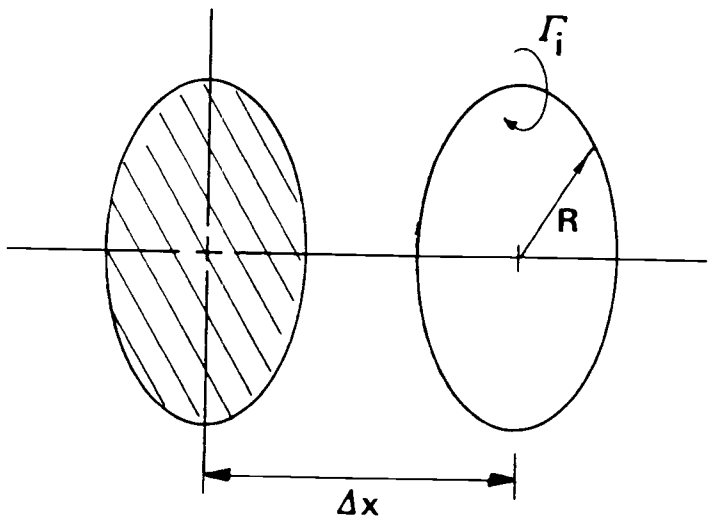

Figure 2.12 Ring Geometry

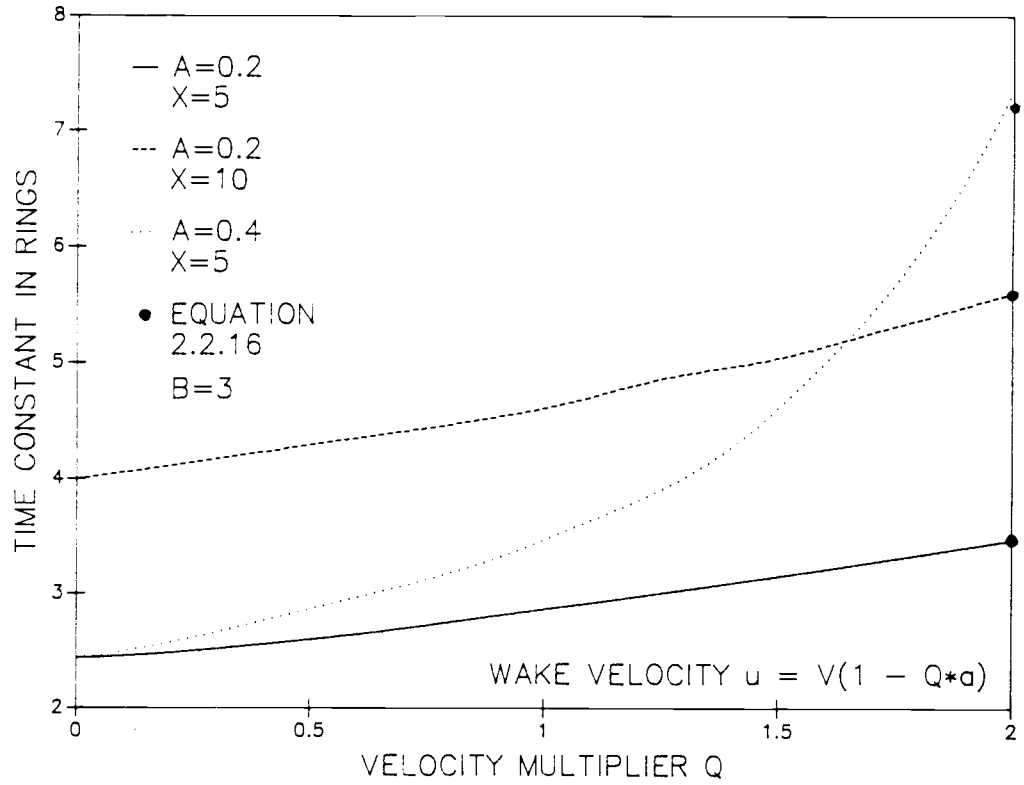

Figure 2.13 Time Constant Variation with Wake Velocity

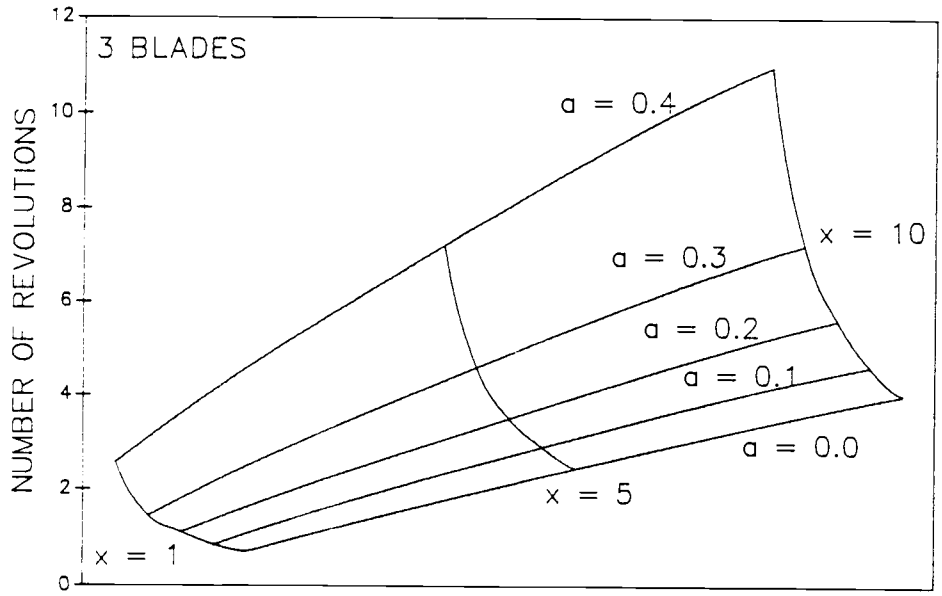

Figure 2.14 Induced Velocity Time Constant for Convective Model with 3-Blade Rotor

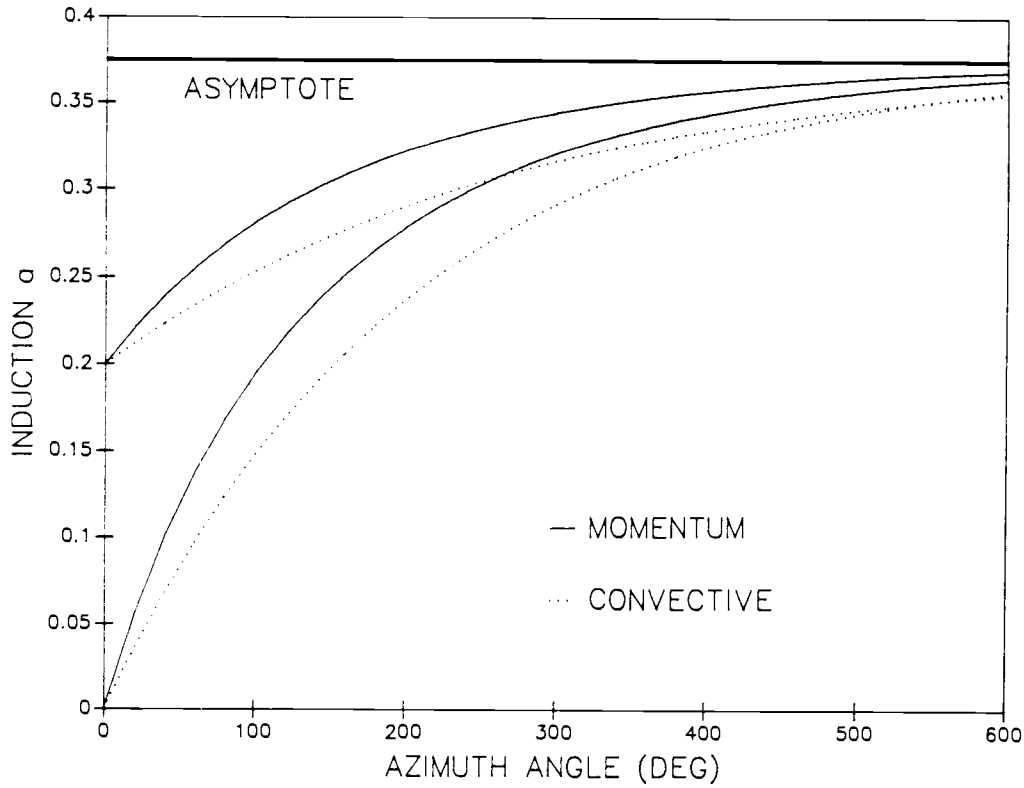

Figure 2.15 Induced Velocity Growth Comparison of Momentum and Convective Methods

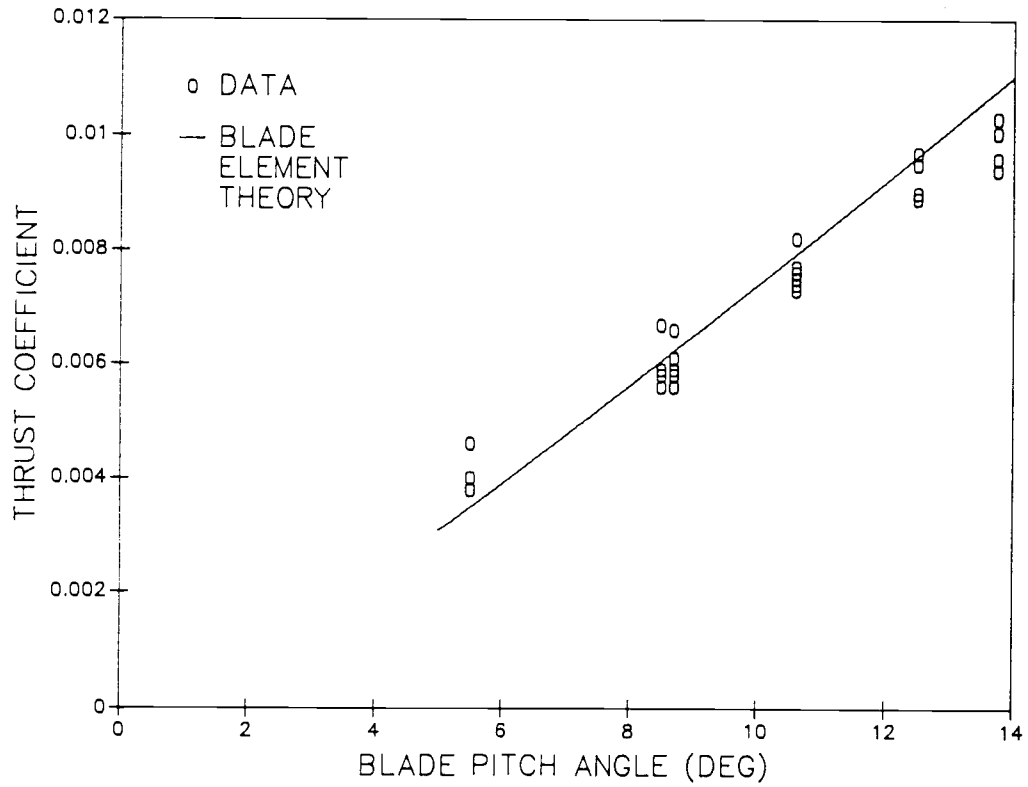

Figure 2.16 A Comparison of Measured and Calculated Thrust Coefficient for a Hovering, Single-Blade Rotor

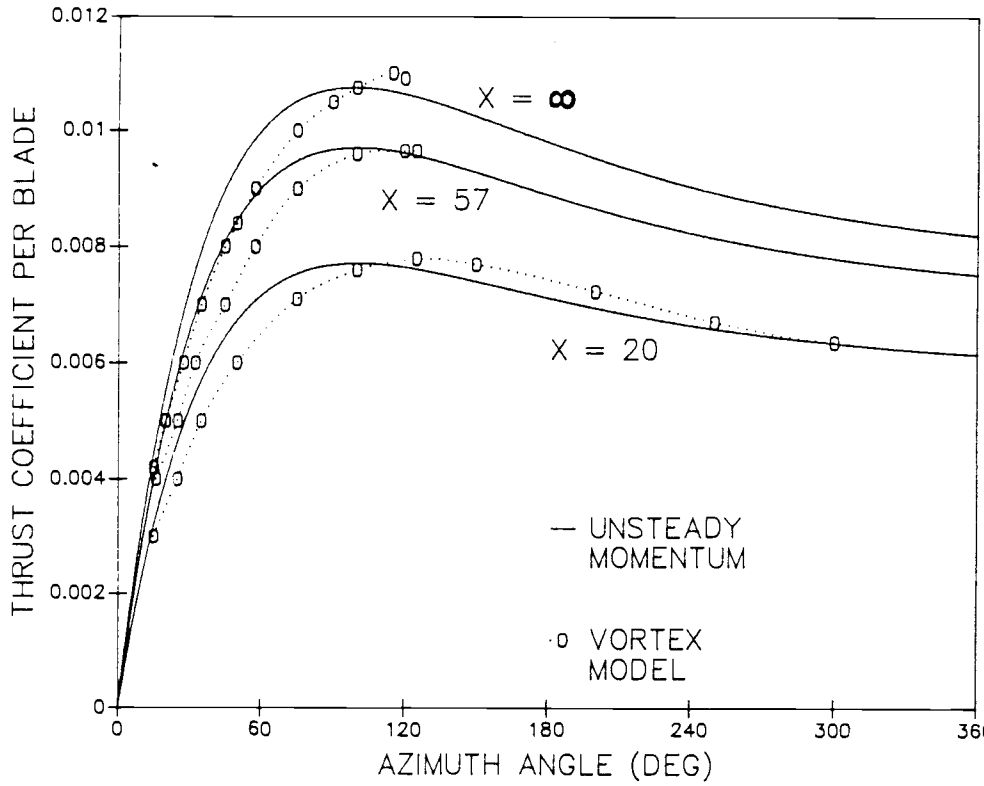

Figure 2.17 Comparison of Summa's Vortex Model with Unsteady Momentum for an Impulsively Started Rotor

2.4 References

1. Glauret, H., "The Analysis of Experimental Results in Windmill Brake and Vortex Ring States of an Airscrew," Reports and Memoranda, No. 1026, 1926.

2. Glauret, H., "On Contraction of the Slipstream of an Airscrew," ARC Reports and Memoranda, No. 1067, 1926.

3. Gohard, J.D., "Free Wake Analysis of Wind Turbine Aerodynamics," MIT Aeroelastic and Structures Lab, Cambridge, MA, TR 184-14, September 1978.

4. Wilson, R.E. and Walker, S.N., "Performance Analysis of Horizontal Axis Wind Turbines," NASA-NAG-3-278, September 1984.

5. Prandtl, L., Gottinger Nachr., p. 193, Appendix, 1919.

6. von Karman, T. and Sears, W., "Airfoil Theory for Non-Uniform Motion," J. Aero. Sci., Vol. 5, No. 10, 1978.

7. Wilson, R.E. et. al., "Aerodynamic Loads on a Darrieus Rotor Blade," J. Fluids Eng., Vol. 105, March 1983.

8. Theodorsen, T., "General Theory of Aerodynamic Instability and the Mechanism of Flutter," NACA TR 496, 1935.

9. Loewy, R.G., "A Two Dimensional Approximation to the Unsteady Aerodynamics of Rotary Wings," J. Aero. Sci., Vol. 24, No. 2, 1957.

10. Venkatesan, C. and Friedmann, P.P., "New Approach to Finite-State Modeling of Unsteady Aerodynamics," AIAA J., Vol. 24, No. 12, 1986.

11. Dinyavari, M.A.H. and Friedmann, P.P., "Application of Time-Domain Aerodynamics to Rotary Wing Aeroelasticity," AIAA J., Vol. 24, No. 9, 1986.

12. Montgomerie, B., "Unsteady Aerodynamics Applied to Horizontal Axis Wind Turbine Disk," National Aeronautical Laboratory, Sweden, FFA Memo, November 1984.

13. Graber, A. and Rosen, A., "Velocities Induced by Semi-Infinite Helical Vortex Filaments," J. Aircraft, Vol. 24, No. 5, 1987.

14. Carpenter, P.J. and Fridovitch, B., "Effect of Rapid Pitch Increase on the Thrust and Induced Velocity Response of a Full Scale Helicopter Rotor," NACA TN 3044, 1953.

15. Peters, D.A., "Hingeless Rotor Frequency Response with Unsteady Inflow," AHS/NASA-Ames Specialists' Meeting on Rotorcraft Dynamics, February 13-15, 1974.

16. Batchellor, G.K., An Introduction to Fluid Dynamics, Cambridge University Press, 1967.

17. Oye, S., "Unsteady Wake Effects Caused by Pitch-Angle Changes," Aerodynamics of Wind Turbines Symposium, Technical Univ. of Denmark, October 1986.

18. Gray, R.B. and Brown, G.W., "A Vortex-Wake Analysis of a Single Blade Hovering Rotor and a Comparison with Experimental Data," AGARD-CP-111, 1972.

19. Summa, J.M., "Potential Flow about Three Dimensional Streamlined Lifting Configurations with Applications to Wings and Rotors," AFOSR-TR-74-1914, 1974.

CHAPTER 3

DETERMINATION OF BLADE LOADS

The formulation of the mathematical model for the determination of blade loads was governed by the decision to limit the analysis to wind turbines of relatively simple rotor geometry without a teetering hub or yaw degree of freedom. The blades were assumed to be flexible with a rigid hub attachment and a single bending degree of freedom about the flapping axis. The tower was assumed to be flexible with a single degree of freedom in the axial direction only. Rotor rotation rate is constant and the rotor plane is assumed to be upwind of the tower. The aerodynamic loading is determined assuming nonlinear lift-drag characteristics in conjunction with modified strip theory to account for wake expansion. The unsteady momentum and wake convection theories described in Chapter 2 form the basis for loading calculations. The calculation sequence is such that the aerodynamic loads are calculated assuming that the blades are in the undeformed position. This assumption is justified since small deflections of the blade geometry will not greatly affect lift and drag calculations. When the aerodynamic loads have been determined, the blade and tower equations of motion are solved to yield velocity and acceleration. The bending moments, shear and tension forces are then calculated by integrating along the deformed blade.

The derivation of the equations solved is presented in this chapter.

3.1 Geometry and Coordinate Transformations

The coordinate system definition for the rigid blade is given in Figure 3.1 where

$\mathbf{n}_i$, (i=1,3) = inertial coordinates

$\mathbf{d}_i$, (i=1,3) = non-rotating translating coordinates

$\mathbf{c}_i$, (i=1,3) = rotating rotor coordinates

$\mathbf{b}_i$, (1=1,3) = rigid blade coordinates

$\mathbf{b}_1$ = normal direction
$\mathbf{b}_2$ = radial direction
$\mathbf{b}_3$ = tangential direction

The two coordinate rotations of the rigid blade coordinates are the rotation of $\mathbf{c}$ in $\mathbf{d}$ of the azimuth angle about the $\mathbf{n}_1$ axis and the rotation of $\mathbf{b}$ about the $\mathbf{c}_3$ axis the preconing angle ψ_0. The resulting coordinate transformation from the blade coordinate to the inertial frame is given by

$$\begin{Bmatrix} \mathbf{n}_1 \\ \mathbf{n}_2 \\ \mathbf{n}_3 \end{Bmatrix} = \begin{bmatrix} \cos\psi_0 & -\sin\psi_0 & 0 \\ \cos\theta\sin\psi_0 & \cos\theta\cos\psi_0 & -\sin\theta \\ \sin\theta\sin\psi_0 & \sin\theta\cos\psi_0 & \cos\theta \end{bmatrix} \begin{Bmatrix} \mathbf{b}_1 \\ \mathbf{b}_2 \\ \mathbf{b}_3 \end{Bmatrix} \qquad (3.1.1)$$

The transformation from the rigid blade coordinates to the deformed blade can be viewed as an additional rotation about the $\mathbf{c}_3$ axis in the opposite direction of the preconing since

blade deflection is defined as positive upwind and preconing is defined as positive downwind. Assuming small blade deflections and linearizing $\sin(\epsilon) = \epsilon$ and $\cos(\epsilon) = 1$, the net slope of the blade can be expressed as the difference between slope due to flexing and slope due to preconing as

$$\psi = \epsilon - \psi_0 \tag{3.1.2}$$

Then defining the normal, radial, and tangential blade coordinates as **n**, **r**, and **t**, respectively, the transformation to the inertial coordinates becomes

$$\begin{Bmatrix} \mathbf{n}_1 \\ \mathbf{n}_2 \\ \mathbf{n}_3 \end{Bmatrix} = \begin{bmatrix} \cos\psi & -\sin\psi & 0 \\ \cos\theta\sin\psi & \cos\theta\cos\psi & -\sin\theta \\ \sin\theta\sin\psi & \sin\theta\cos\psi & \cos\theta \end{bmatrix} \begin{Bmatrix} \mathbf{n} \\ \mathbf{r} \\ \mathbf{t} \end{Bmatrix} \tag{3.1.3}$$

3.2. Blade Deflection

The flexing of each blade is modeled as a single degree of freedom in the direction normal to the blade rotational plane using and assumed mode shape. Blade deflection in the tangential direction is assumed to be zero (rigid) and deflection in the radial direction can be expressed in terms of the normal deflection for small displacements. In the normal direction, deflection of the i^{th} blade is given by the product of a single assumed mode shape function and a function of time given by

$$\delta_{ni}(r,t) = S(r) \cdot q_i(t), \quad i=1,3 \qquad (3.2.1)$$

where $S(r)$ = bending mode shape, a function only of distance along blade coordinate r

$q(t)$ = blade displacement, a function time

$\delta_t = 0$

$\delta_{ri} = f(\delta_{ni})$

For a small blade deflection as shown in Figure 3.2, the radial deflection for a given blade can be expressed by

$$\delta_r = r - \int_0^r \cos(d\delta_n/dr)\, dr$$

substituting

$$\cos(d\delta_n/dr) = 1 - 2\sin^2(d\delta_n/dr) \quad 1 - \tfrac{1}{2}(d\delta_n/dr)^2$$

then for small deflections, the radial deflection is

$$\delta_r = -\int_0^r (dS(r)/dr)^2\, dr \cdot \{q_i(t)\}^2$$

The choice of the shape function to be used is governed by the boundary conditions for the blade. The function chosen for this analysis is

$$f(z) = (z^4 - 4z^3 + 6z^2)/3 \qquad (3.2.2)$$

where z is the dimensionless distance along the flexible portion of the blade given by

$$z = (r - r_H)/(R - r_H)$$

where r = radial distance
r_H = hub radius
R = tip radius

For a cantilever blade the boundary conditions that must be met are:

$f = 0 \quad @ \quad z = 0$ (no deflection at $r = r_H$)
$df/dz = 0 \quad @ \quad z = 0$ (no slope at $r = r_H$)
$d^2f/dz^2 = 0 \quad @ \quad z = 1$ (no moment at $r = R$)
$d^3f/dz^3 = 0 \quad @ \quad z = 1$ (no shear at $r = R$)

The slope of the blade used for coordinate transformations is given by

$$\epsilon = \partial \delta_n / \partial r = dS(r)/dr \cdot q(t) \qquad (3.2.3)$$

The fourth degree of freedom q_4 is the tower displacement in the axial direction and is modeled as the mass-spring system pictured in Figure 3.3. Approximating the tower as a cantilever beam, the equivalent tower tip mass m_{tip} represents the nacelle mass, rotor, and some fraction of the tower mass. The spring constant k_{eq} represents the equivalent spring constant for the cantilever tower which can be determined from tower material and geometry using

$$k_{eq} = 3EI/L^3 \qquad (3.2.5)$$

or, can be found from a measured tower natural frequency.

3.3. Blade Kinematics

The derivation of the blade equations of motion and the extraction of blade forces require expressions for the velocity and acceleration of an arbitrary point Q on the i^{th} deformed blade. A position vector can be given as

$$({}^{N}\mathbf{p}^{Q})_i = q_4\mathbf{n}_1 + \delta_{ni}\mathbf{b}_1 + (r+\delta_{ri})\mathbf{b}_2 \qquad (3.3.1)$$

where ${}^{N}\mathbf{p}^{Q}$ is the position of point Q in the inertial reference frame **n** and the displacements δ_n and δ_r are given in equations 3.2.1 and 3.2.2, respectively. From this expression, the velocity of point Q is the time derivative of ${}^{N}\mathbf{p}^{Q}$ in the inertial frame **n**. This is found by

$${}^{N}\mathbf{v}^{Q} = {}^{N}\,d/dt({}^{N}\mathbf{p}^{Q})$$

This can be expressed in the rigid blade coordinates as

$$({}^{N}\mathbf{v}^{Q})_i = v_1\mathbf{b}_1 + v_2\mathbf{b}_2 + v_3\mathbf{b}_3 \qquad (3.3.2)$$

where
$$v_1 = \dot{\delta}_{ni} + \dot{q}_4\cos\psi_0$$
$$v_2 = \dot{\delta}_{ri} - \dot{q}_4\sin\psi_0$$
$$v_3 = \Omega[\delta_{ni}\sin\psi_0 + (r+\delta_{ri})\cos\psi_0]$$

In the same way, the acceleration of point Q is defined by

$${}^{N}\mathbf{a}^{Q} = {}^{N}\,d/dt({}^{N}\mathbf{v}^{Q})$$

This can be expressed in terms of the rigid blade coordinates as

$$({}^{N}\mathbf{a}^{Q})_i = a_1\mathbf{b}_1 + a_2\mathbf{b}_2 + a_3\mathbf{b}_3 \qquad (3.3.3)$$

where $a_1 = \dot{v}_1 - \Omega v_3 \sin\psi_0$

$a_2 = \dot{v}_2 - \Omega v_3 \cos\psi_0$

$a_3 = \dot{v}_3 + \Omega(v_2 \cos\psi_0 + v_1 \sin\psi_0)$

and $v_1 = \ddot{\delta}_{ni} + \ddot{q}_4 \cos\psi_0$

$v_2 = \ddot{\delta}_{ri} - \ddot{q}_4 \sin\psi_0$

$v_3 = \Omega[\dot{\delta}_{ni} \sin\psi_0 + \dot{\delta}_{ri} \cos\psi_0]$

3.4. Aerodynamic Loads

The aerodynamic calculations described in Chapter 2 yield results for the lift coefficient, C_L, and the drag coefficient, C_D, at each blade station for each azimuth angle increment. The lift and drag forces per unit length of blade can now be calculated as

$$\text{lift/unit length} - L = \tfrac{1}{2}\rho W^2 c C_L \qquad (3.4.1)$$

$$\text{drag/unit length} - D = \tfrac{1}{2}\rho W^2 c C_D \qquad (3.4.2)$$

The wind velocity W in these equations represents the relative wind equal to the sum of free-stream velocity in the blade coordinates plus the blade velocity given by equation 3.3.2. These forces are now resolved into the rigid blade coordinates normal and tangential to the blade plane. Referring to the geometry defined in Figure 2.4, and using the coordinate descriptions of Figure 3.1, the aerodynamic forces integrated over the blade length are given as

$$F_A = \int_0^R (f_1 \mathbf{b}_1 + f_2 \mathbf{b}_2 + f_3 \mathbf{b}_3) dr \qquad (3.4.3)$$

where $f_1 = -L \cos\phi - D \sin\phi$

$f_2 = 0$

$f_3 = L \sin\phi - D \cos\phi$

3.5. Equations of Motion

The equations of motion are formulated for a discretized blade so that kinematics and forces are evaluated at points along the blade and integrated numerically along the blade length. The equations were obtained using the methods of Kane and Levison [1], which gives the equation of motion in the form

$$F_r + F_r^* = 0 \qquad (3.5.1)$$

where, F_r = generalized active force

F_r^* = generalized inertia force

The subscript r refers to the number of generalized coordinates. In this analysis, r = 1, 2, and 3 are reserved for the three blade deflections and r = 4 is the tower deflection. The generalized active and inertia forces can be obtained from expressions of potential and kinetic energy, respectively, or can be obtained using the blade

kinematics. The generalized active force is determined from blade kinematics using

$$F_r = \mathbf{v}_r^Q \cdot \mathbf{R} \qquad r=1,n \qquad (3.5.2)$$

where, $\mathbf{v}_r^Q$ = holonomic partial velocity of point Q

$\mathbf{R}$ = resultant of external forces including aerodynamic forces and gravity loading

When the external forces acting on the blade are conservative, a potential energy function can be constructed and the generalized active force is found by

$$F_r = -\partial V/\partial q_r \qquad r=1,n \qquad (3.5.3)$$

The nonconservative forces, which in this analysis are the aerodynamic forces acting on the blade must be determined using equation 3.5.2.

The generalized inertia forces are determined using blade kinematics from

$$F_r^* = \mathbf{v}_r^Q \cdot (-m\mathbf{a}^Q) \qquad r=1,n \qquad (3.5.4)$$

where, $\mathbf{a}^Q$ = acceleration of Q, equation 3.3.3.

m = mass per unit length of element = μA

For systems that are holonomic and where the generalized speeds $u_r = \dot{q}_r$, then the generalized inertia force can be obtained from the kinetic energy function K_E by

$$F_r^* = -d/dt[\partial K_E/\partial \dot{q}_r] - \partial K_E/\partial q_r \qquad r=1,n \qquad (3.5.5)$$

Defining the generalized speeds as $u_r = \dot{q}_r$, r = 1,4 the partial velocities can be found from the expression for blade velocity, equation. 3.3.2.

$$\mathbf{v}_r^Q = S(r)\mathbf{b}_1 - \tfrac{1}{2}\int_0^R (dS(r)/dr)dr\mathbf{b}_2 + S(r)\sin\psi_0\mathbf{b}_3 \qquad r=1,n \tag{3.5.6}$$

$$\mathbf{v}_4^Q = \cos\psi_0\mathbf{b}_1 - \sin\psi_0\mathbf{b}_2 \tag{3.5.7}$$

Potential functions can be written of the conservative gravitational and elastic forces. The potential functions for the elastic and gravitational forces are given by

$$(V_g)_r = \int_0^R \mu A(r + \delta_r)\sin\theta dr \qquad r=1,3 \tag{3.5.8}$$

$$(V_g)_4 = 0 \tag{3.5.9}$$

$$(V_e)_r = \tfrac{1}{2}\int_0^R EI(r)(\partial^2\delta_n/\partial z^2)^2 dz \qquad r=1,3 \tag{3.5.10}$$

$$(V_e)_4 = \tfrac{1}{2}k_{EQ}q_4^2 \tag{3.5.11}$$

then the generalized active forces are found from 3.5.3. The generalized active forces from the nonconservative aerodynamic excitation and damping forces are found using 3.5.2, 3.5.6, 3.5.7, and the partial velocities 3.4.3.

The generalized inertia forces for this system are found from the kinetic energy functions using. The kinetic energy is defined by

$$K_E = \tfrac{1}{2}\int_0^R \mathbf{v}^Q \cdot \mathbf{v}^Q \, dm \qquad (3.5.12)$$

Using the velocity from 3.3.2 , the kinetic energy of the system becomes

$$K_E = \tfrac{1}{2}\int_0^R \mu A(v_1^2 + v_2^2 + v_3^2)dr + \tfrac{1}{2}m_{TIP}\,\dot{q}_4^2 \qquad (3.5.13)$$

Expanding this term, neglecting terms on the order r^2, and using 3.5.5 yields expressions for F_r^*. Combining the generalized active and inertia forces using 3.5.1. gives the set of four simultaneous differential equations of motion for the coupled blade-tower motion in the form

$$[m]\{q\} + [k]\{q\} = \{Q\} \qquad (3.5.14)$$

where

$$m_{ii} = \int_0^R \mu A[S(r)^2 - \int_0^r (dS/dr)^2 dr \sin\psi_0]dr \qquad i=1,3$$

$$m_{44} = B\int_0^R \mu A dr + m_{TIP}$$

$$m_{i4} = m_{4i} = \int_0^R \mu A S(r) dr \cos\psi_0 \qquad i=1,3$$

$$k_{ii} = \int_0^R EI(d^2S/dr^2)^2 dr +$$

$$\Omega^2\int_0^R \mu A[-S(r)^2\sin^2\psi_0 + r\int_0^r (dS/dr)^2 dr \cos\psi_0]dr \qquad i=1,3$$

$$k_{44} = k_{eq}$$

$$Q_i = \int_0^R (f_{1i} + \sin\psi_0 f_{3i}) S(r)\,dr + \Omega^2 \int_0^R \mu Ar S(r)\,dr \sin\psi_0 \cos\psi_0 \qquad i=1,3$$

$$Q_4 = \sum_{i=1}^{3} \int_0^R (\cos\psi_0 f_{1i} - \sin\psi_0 f_{3i})\,dr$$

3.6. Loads Calculations

The loads of interest are the shear loads in directions normal and tangential to the blade and flapwise an edgewise bending moments. These loads are evaluated on the deformed blade by numerical integration of the aerodynamic and inertial loads along from the tip to the rotor axis. Choosing a blade element as shown in Figure 3.4, the normal and tangential shear forces at the left end of the element are given by

$$(V_1)_m = (V_1)_n + \int_m^n (\mu A a_1 - f_1)\,dr \qquad (3.6.1)$$

$$(V_3)_m = (V_3)_n + \int_m^n (\mu A a_3 - f_3)\,dr \qquad (3.6.2)$$

the tension along the blade is

$$T_m = T_n - \int_m^n \mu A a_2 dr \qquad (3.6.3)$$

The flapwise bending moment about the $\mathbf{b}_3$ axis

$$(M_3)_m = (M_3)_n - (V_1)_n(r_n-r_m) - T_n(r_n-r_m)\psi$$

$$- \int_m^n r(\mu A a_1 - f_1)dr + \int_m^n r\mu A a_2 dr \qquad (3.6.4)$$

and the edgewise bending moment about the $\mathbf{b}_1$ axis

$$(M_1)_m = (M_1)_n + (V_3)_n(r_n-r_m) + \int_m^n r(\mu A a_3 - f_3)dr \qquad (3.6.5)$$

3.7. Wind Models

The models that provide a wind input to each blade station in the rotor plane for assessment of aerodynamic loads include corrections for wind shear, tower interference, fixed yaw of the rotor plane, and wind turbulence for estimation of stochastic loads. A brief description of the algorithms used is presented.

3.7.1 Wind Shear

Wind shear is typically the cause of the largest cyclic baled excitation having a frequency of one cycle per

revolution. Wind shear is also related to the turbulence length scale and has some influence on turbulence loads at other frequencies. One conventional model for wind shear is given in the form of a power law expression by

$$\frac{V}{V_{HUB}} = \left(1 + \frac{z}{z_{HUB}}\right)^{n} \qquad (3.7.1)$$

The shear exponent is typically near the fraction 1/7, but depends on the ground roughness and topography. If meteorological data exist at the site, a better correlation for n can be determined.

Another model uses a logarithmic wind shear. The form of the equation in this case is

$$\frac{V}{V_{HUB}} = \frac{\ln(z/z_0)}{\ln(z_{HUB}/z_0)} \qquad (3.7.2)$$

where z_0 is a parameter known as the surface roughness length of the site. As with the power law model, the surface roughness length is dependent on ground conditions upwind of the turbine. Proposed relationships between the power law exponent and the surface roughness length are discussed in section 3.7.3.

3.7.2 Tower Interference

Tower interference in the flowfield of the wind turbine can be caused by the tower wake if the rotor plane is

downwind of the tower, or by a blockage when the rotor is upwind of the tower.

Wake Model for a Downwind Rotor

The wake model used for a downwind machine is based on the conservation of momentum, where the deficit in momentum flux is equated to the drag force on the tower. The velocity deficit can then be calculated for an assumed velocity profile in the wake. Figure 3.6 shows the selected control surface for application of conservation of momentum given in integral form for steady state conditions as

$$\mathbf{F} = \iint_{CS} \mathbf{v}\cdot(\mathbf{v}\cdot\mathbf{n})\,dA \qquad (3.7.3)$$

Selecting a velocity distribution in the form of a $(\text{cosine})^2$ function , the wind velocity profile assuming a deficit width of two tower diameters is of the form

$$\frac{V(y)}{V_\infty} = 1 - e\cos^2\left(\frac{\pi y}{2d}\right) \qquad (3.7.4)$$

The peak velocity deficit e can be found in terms of the drag coefficient as

$$e = (2/3)[1 - (1-3C_D/2)^{\frac{1}{2}}] \qquad (3.7.5)$$

Blockage Model for an Upwind Rotor

A model of the tower interference or blockage affect of an upwind rotor can be formulated from potential flow theory for simple incompressible flow about a cylinder. In a previous analysis of the Howden wind turbine also used for comparison in this report, this simple approach was used. In their report, the authors found that the simple potential flow model gave a velocity profile that appeared to be too severe and modified the blockage by arbitrarily reducing the peak and increasing the azimuth span of the effect. The approach taken for the present model is somewhat heuristic, yet yields a similar result while additionally accounting for the presence of the wake downstream of the tower.

Referring to Figure 3.7, the model begins with simple flow about a cylinder which can be expressed in terms of a complex potential as

$$W_C(z) = V_\infty[ze^{-i\zeta} + (\frac{d^2}{4z})e^{i\zeta}] \qquad (3.7.6)$$

Noting that the conjugate velocity can be found by

$$\tilde{v} = \frac{dW}{dz} \qquad (3.7.7)$$

the velocity in the flowfield at a point z = x+iy is

$$(v/V_\infty)_C = \{\cos\zeta - \frac{d^2}{4(x^2+y^2)^2}[(x^2-y^2)\cos\zeta + 2xy\sin\zeta]\}$$

$$-i\{\sin\zeta + \frac{d^2}{4(x^2+y^2)^2}[(x^2-y^2)\sin\zeta - 2xy\cos\zeta]\} \qquad (3.7.8)$$

The model for the flow about a cylinder has two deficiencies; it does not account for the turbulent wake behind the tower and at a large distance from the tower, $(v/U) > 1$, which is physically impossible. A way to resolve these problems is to superimpose the flow about a source located at the center of the cylinder. For flow about a source, the complex potential is given by

$$W_S(z) = V_\infty z e^{-i\zeta} + \left(\frac{q}{2\pi}\right)\ln(z) \qquad (3.7.9)$$

where the strength of the source is chosen to give a wake width equal to the tower width, i.e. $q = dU$. Figure 3.8 shows schematically the effect of this flow superposition. The velocity distribution of the source is

$$(v/V_\infty)_S = \left\{\cos\zeta + \frac{dx}{2\pi(x^2+y^2)}\right\} - i\left\{\sin\zeta + \frac{dy}{2\pi(x^2+y^2)}\right\} \qquad (3.7.10)$$

The average velocity of the superimposed flows is

$$(v/V_\infty)_{AVG} = \tfrac{1}{2}[(v/V_\infty)_C + (v/V_\infty)_S]$$

The projection of the flow velocity in the direction of the wind is found to be

$$(v/V_{\infty})_{WIND} = 1 + \frac{d(x\cos\zeta + y\sin\zeta)}{4\pi(x^2+y^2)} - \frac{d^2[(x^2-y^2)\cos 2\zeta + 2xy\sin 2\zeta]}{8(x^2+y^2)^2} \qquad (3.7.11)$$

Figure 3.9 gives a comparison of the resulting velocity distributions for potential flow about a cylinder and the superimposed flow pattern. The superimposed flow, while by no means a rigorous model of the actual flow gives qualitatively better results than simple flow about a cylinder.

3.7.3 Turbulence Models

A turbulent wind simulation model is used to evaluate the stochastic load response of the blades. The selection of which of the existing models available was influenced by the size constraints of a PC based system for which this work was directed and a comparison of some of the models in the public domain. The code used in this work is the rotational wind code developed by Connell and others [2,3] at the Pacific National Laboratory.

The input to the turbulence model that determines the characteristic of the wind is the surface roughness length z_0. For predictive analysis, where the loads are to be analyzed for a site where wind conditions are not well defined, the surface roughness length is estimated from a

description of the local terrain. Guidelines have been published [4,5] that give representative values of surface roughness for a range of general terrain categories. Values in Table 3.1 from Frost are typical. If some data exist on wind conditions at a site, other methods may be used. For example, if data on the local value of wind shear exist, the surface roughness length can be found by obtaining the best fit to equation 3.7.3. Frost published a graph reproduced in Figure 3.10 that estimates the surface roughness length from the power law exponent. For the predictions given in Chapter 4, the method of obtaining the roughness length was to calculate the turbulence intensity from the hub height wind speed channel using the relationship given by Counihan as

$$I = 1 \; / \; \ln\left(\frac{z_{HUB}}{z_0} \right) \qquad (3.7.12)$$

where I is the fractional turbulence intensity. Using the example of the Howden machine that has a hub height z_{HUB} of 24.1 meters and a measured hub height turbulence intensity of 17% (I=0.17), the estimated surface roughness length z_0 is 0.067 meters. The sensitivity of the magnitude of predicted loads to the estimate of surface roughness length is examined in Chapter 4.

3.8 Numerical Solution Methods

The numerical solution of the equations of motion is accomplished using an Adams predictor-corrector method. This formulation uses the fourth-order Adams-Bashforth formula as a predictor and the fourth order Adams-Moulton formula for a corrector. Error is estimated from the procedure with a corrector modifier of the form

$$\text{ABS(Error)} = \frac{19}{270} (Y_P - Y_C)$$

The predictor-corrector multistep methods are not self starting, therefore a fourth order Runga-Kutta method was employed to generate the first three points [6].

Integration along the blade to determine elements of the mass and stiffness matrices uses simple trapezoidal integration, as does integration to determine loads. The solution first order differential equations that are generated from the approximate unsteady aerodynamic models, equations 2.2.10, 2.2.18, and 2.2.21, are solved using fourth-order Runga-Kutta techniques.

Table 3.1 Typical Values of Surface Roughness Length for Various Types of Surfaces

Type of Surface	z_0 (m)
Mud Flats, Ice	$1 \times 10^{-5} - 3 \times 10^{-5}$
Smooth Sea	$2 \times 10^{-4} - 3 \times 10^{-4}$
Sand	$1 \times 10^{-4} - 1 \times 10^{-3}$
Snow Surface	$1 \times 10^{-3} - 6 \times 10^{-3}$
Mown Grass (0.01 m)	$1 \times 10^{-3} - 1 \times 10^{-2}$
Low Grass, Steppe	$1 \times 10^{-2} - 4 \times 10^{-2}$
Fallow Field	$2 \times 10^{-2} - 3 \times 10^{-2}$
High Grass	$4 \times 10^{-2} - 1 \times 10^{-1}$
Palmetto	$1 \times 10^{-1} - 3 \times 10^{-1}$
Forest and Woodland	$1 \times 10^{-1} - 1$
Suburbia	$1 - 2$
City	$1 - 4$

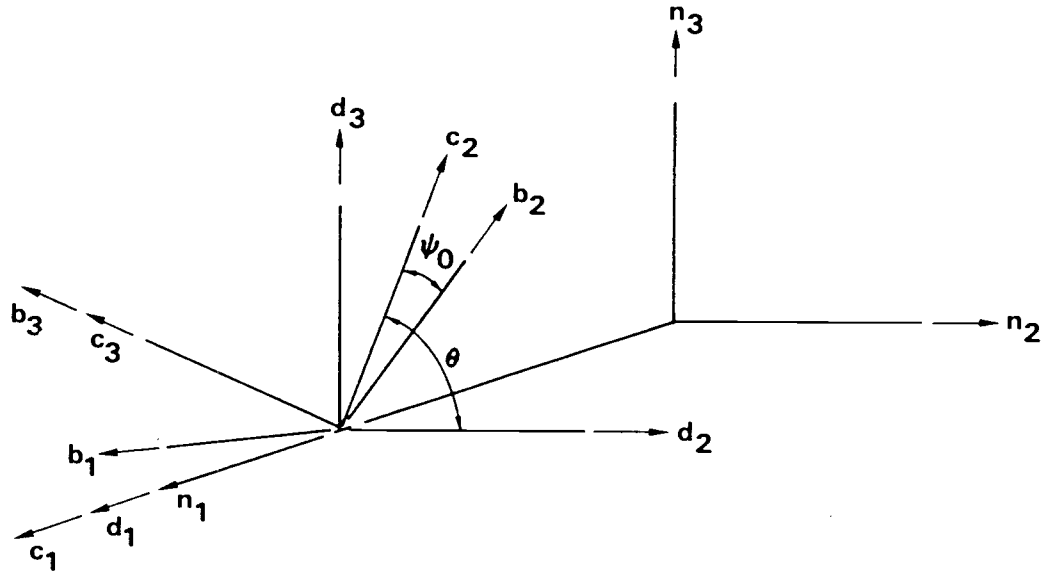

Figure 3.1 Rigid Blade Transformations

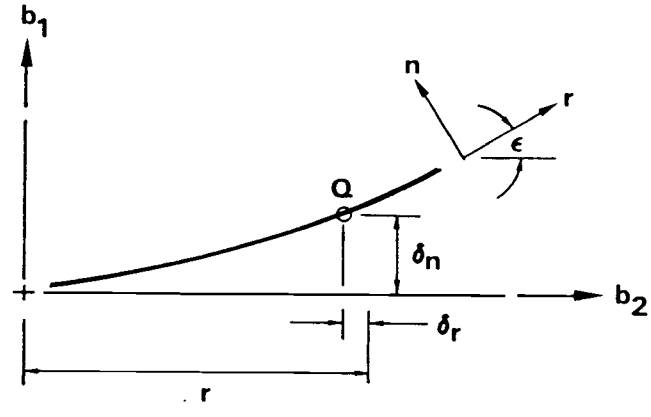

Figure 3.2 Deformed Blade Geometry

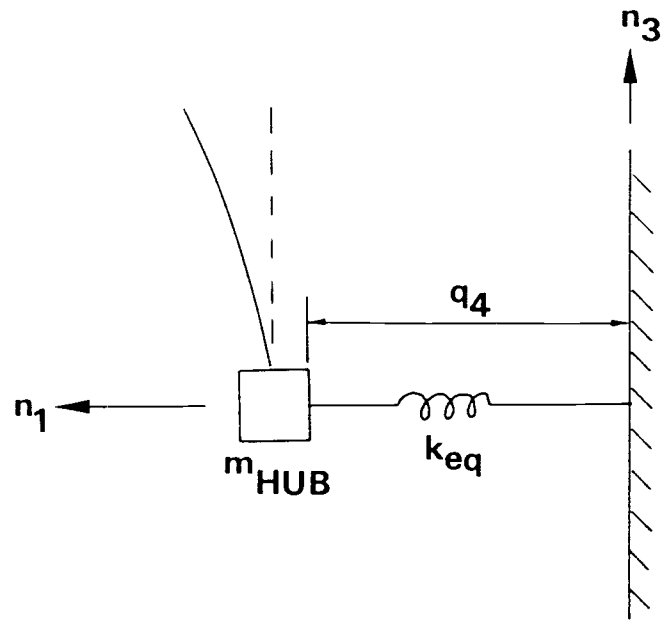

Figure 3.3 Tower Model Schematic

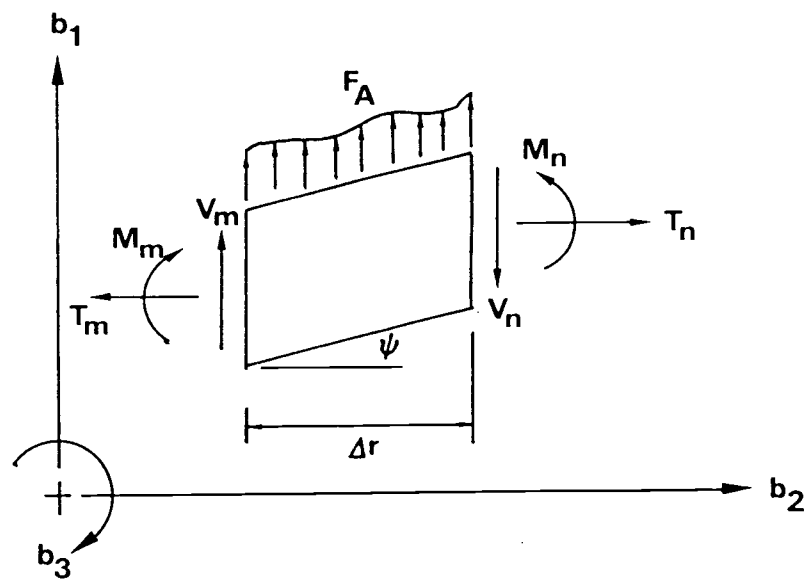

Figure 3.4 Blade Element Definition

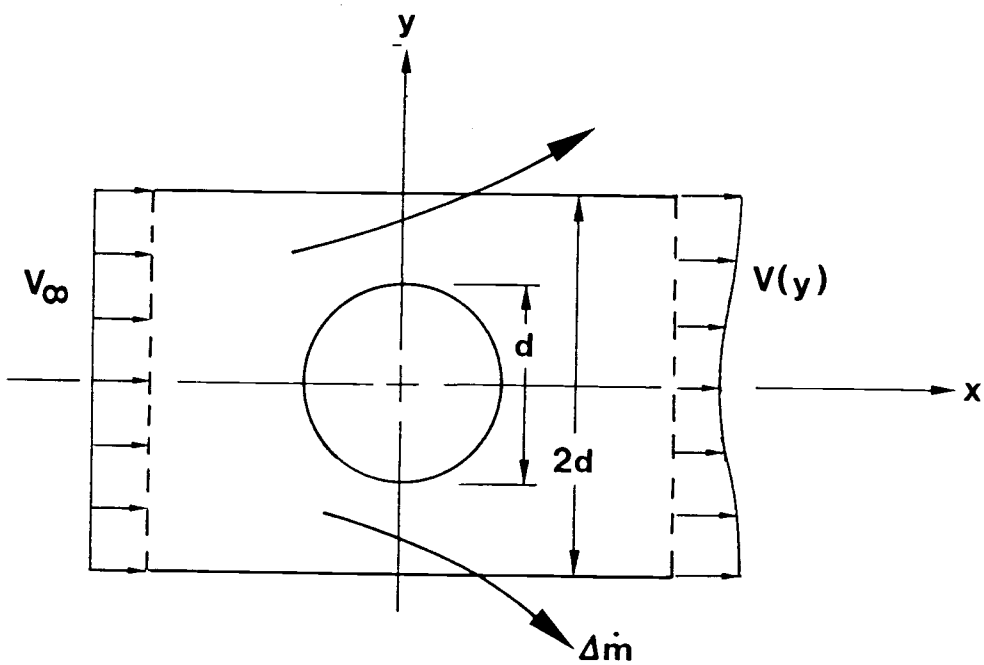

Figure 3.5 Tower Control Volume for Shadow Model

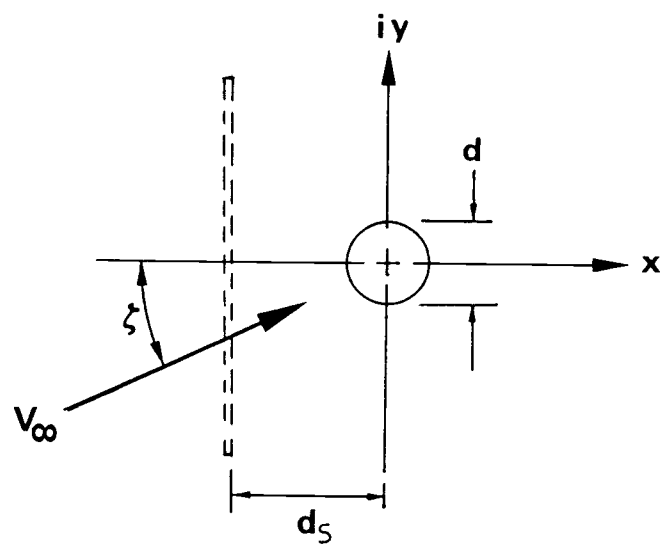

Figure 3.6 Tower Potential Flow Model for Upwind Rotor

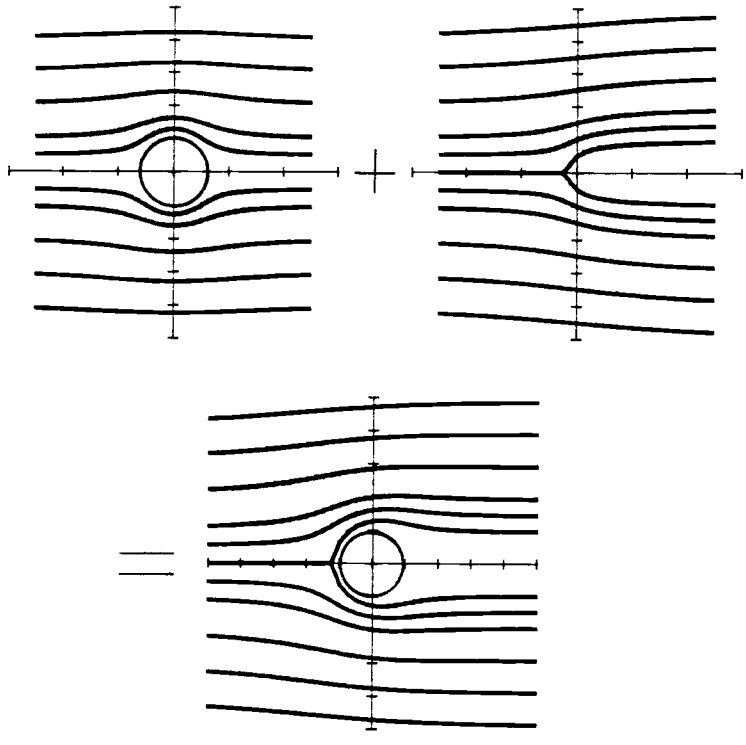

Figure 3.7 Superposition of Flow Models

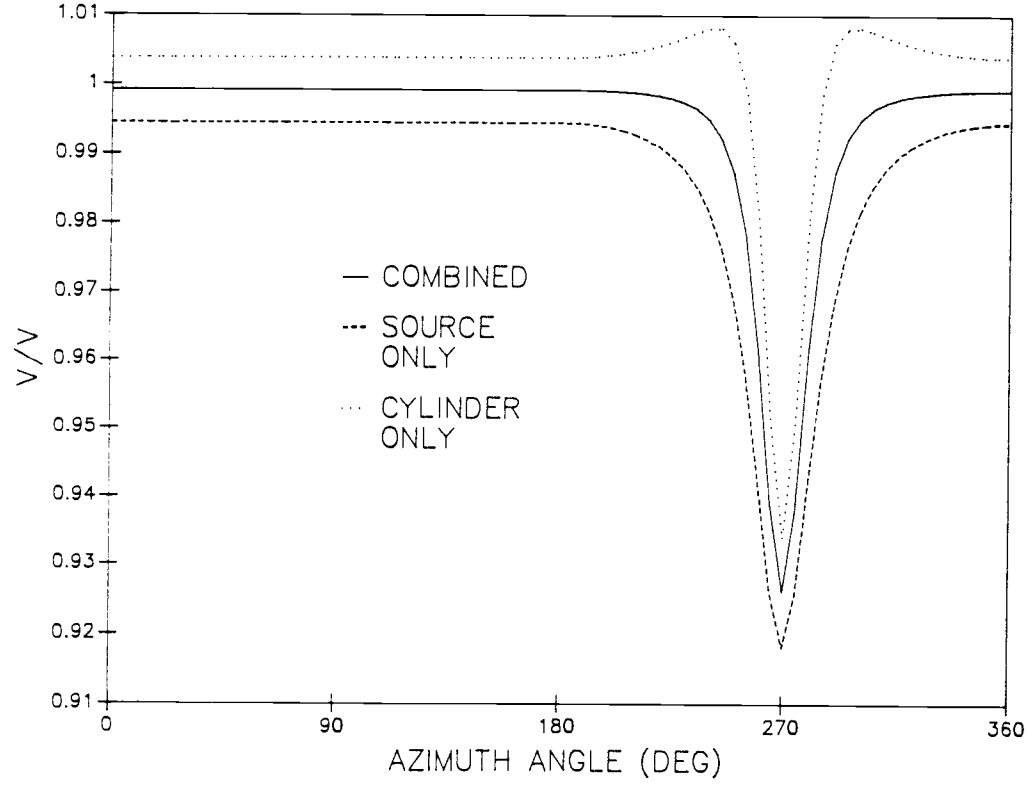

Figure 3.8 Velocity Distribution of an Upwind Rotor

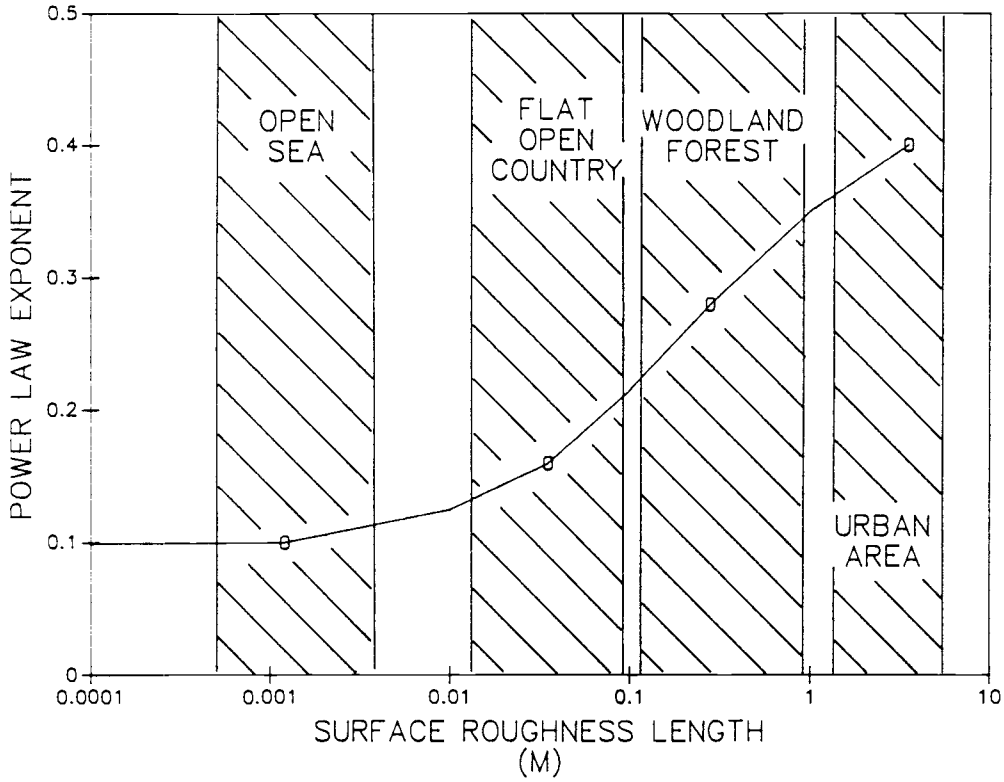

Figure 3.9 Surface Roughness Length vs. Power Law Exponent

3.9 References

1. Kane, T.R. and Levison, D.A., Dynamics: Theory and Applications, McGraw-Hill, Inc., 1985.

2. Connell, J.R., "The Spectrum of Wind Speed Fluctuations by a Rotating Blade of a Wind Energy Conversion System," Solar Energy, Vol. 29, No. 5, pp. 363-375, 1982.

3. Powell, D.C. and Connell, J.R., "A Model for Simulating Rotational Data for Wind Turbine Applications," PNL-5857, April 1986.

4. Frost, W., Long, B.H., and Turner, R.E., "Engineering Handbook on the Atmospheric Environmental Guidelines for Use in Wind Turbine Generator Development," NASA Tech. Paper 1359, 1978.

5. Counihan, J., "Adiabatic Atmospheric Boundary Layers: A Review and Analysis of Data from the Period 1880-1972," Atmospheric Environment, Vol. 9, pp. 871-915, 1975.

6. Gerald, C.F. and Wheatley, P.O., Applied Numerical Analysis, Addison-Wesley, 1984.

CHAPTER 4

MODEL COMPARISON TO TEST DATA

Evaluation of the methods described comes from comparison with test data from a Howden 330 kW horizontal-axis wind turbine located in Palm Springs, CA, and used as part of the SERI/DOE Cooperative Field Test Program. A description of the machine is given in Appendix A. A considerable body of literature exists concerning loads prediction for the Howden machine [1-4] using steady state, linear aerodynamics, so this work extends that analysis to the examination of unsteady aerodynamics and turbulence on loads.

The comparison of loads examines mainly the thrust, torque, and flapwise bending moments, comparing the mean and cyclic loads. Thrust load data was not directly available so the thrust load predictions are checked by using the rotor thrust to calculate tower bending moment which can be compared to data. Predictions were made using both steady and turbulent wind with steady state and unsteady aerodynamics. Additionally, comparisons were made to evaluate the effect of including tower motion in the calculation of the blade dynamics and aerodynamics.

4.1 Mean Loads

The mean loads were extracted from five runs of ten minutes each taken at a sample rate of 42 Hz. The predictions shown for steady wind are the cycle averages taken after the code converged on a solution for blade deflection. Typically, three or four revolutions are sufficient to achieve convergence. When a turbulent wind input is used, the wind velocity predictions from the PNL turbulent wind simulation code are used to drive the loads code. The typical number of revolutions simulated depends on the azimuth angle spacing since the turbulence code generates 2048 points. For a ten degree spacing, this results in approximately 56 complete revolutions. The loads predicted from this simulation are then binned by azimuth angle. The loads code defines zero azimuth angle when the reference blade is in the horizontal position, but the data set has zero azimuth angle in the vertical position. To show a direct comparison of cyclic loads, the data set was shifted to match the model definition. All mean loads were calculated using only one degree of freedom for blade bending with tower motion prohibited since no change in mean loads was found when all four degrees of freedom were included.

Using steady wind, steady state aerodynamics, and the measured blade tip pitch, the power, blade bending moment at two stations, and tower bending moment were predicted for a

range of wind speeds. The results of these predictions are shown compared to data in Figures 4.1 to 4.4, respectively. The rotor power and tower bending moment calculations agree quite well with the data, however the bending moment predictions are approximately 20% low. Similar low results of the predicted bending moments were also reported in [1]. Cases run to evaluate the effect of unsteady aerodynamics, where the only variation in wind velocity is caused by wind shear and tower blockage, showed no change in mean loads. Turbulent wind simulations were also run with steady state and unsteady aerodynamic models. The turbulence simulation with steady state aerodynamics showed no change in mean loads prediction, however the mean loads predictions with turbulent wind and unsteady aerodynamics shows an increase of up to 50% in all loads. A summary of the data from Howden run 12-7 and the predictions at a mean wind speed corresponding to that run is given in Table 4.1 and the resulting bending moment predictions at the 1.5 m and 8.25 m stations are shown in Figures 4.2 and 4.3, respectively. The higher loads predicted for the turbulent wind/unsteady aerodynamics case agree much better with the data than all other predictions shown except in the case of the derived thrust. The increases in mean loads when unsteady aerodynamics are used is caused by the long time constant lag in induced velocity which results in a lower mean level of induction. The lower mean induced velocity translates into high loads since the relative wind is increased. The

effect was not seen to the same degree in torque and thrust loads, but these loads are estimated by multiplying the single blade results times the number of blades and are not representative of the calculations of a multi-blade turbulence code.

4.2 Cyclic Loads

For comparison of cyclic loads, the flapwise bending moments at two stations along the blade at 1.5 m (11.5% of blade radius) and at 8.25 m (63.5% of blade radius) are used. Thrust and torque loads, being the cumulative effect of three blades do not give good resolution of cyclic loads. All calculations presented in this section were performed for a single blade with one flapping degree of freedom and no tower motion.

Using only steady state aerodynamics, cyclic loads were evaluated using both a steady wind and turbulent wind. The results of these predictions are shown at both blade stations in Figures 4.5 and 4.6. At both blade stations, the turbulent wind gives a predicted cyclic bending moment that shows a slight improvement over the steady wind.

The inclusion of unsteady models tends to damp out the cyclic response for frequencies greater than 1p (0.7 Hz) while not changing the magnitude of the 1p variation. Since no yaw is assumed, the main driver for 1p oscillation is the

wind shear with some contribution from large scale turbulence. The drivers for the higher frequencies are the tower blockage, turbulence, and the non-linear portion of wind shear. The high 2p (1.4 Hz) response of the Howden machine is caused by the close correspondence in frequencies between 2p and the resonant frequency of the first bending mode (1.44 Hz). The net effect of the unsteady aerodynamics, both the unsteady momentum and convective formulations, is a smoothing of the cyclic response curve. The cyclic load variation is influenced much more by the shed wake effects which cause a lag in the applied aerodynamic force than by the trailing wake effects which cause a lag in the induced velocity. The reason for this is that the time constant for trailing wake effects is typically greater than one revolution so changes in a time of less than one revolution are not expected. The shed wake on the other hand has a time constant typically less than a quarter of a revolution which causes the smoothing evident in the cyclic loads. The trailing wake lag however influences the mean loads as discussed. Figures 4.7 and 4.8 show comparisons for both blade stations of the cyclic bending moments with turbulent wind input for steady state aerodynamics and unsteady aerodynamics using unsteady momentum. The peak cyclic loads remain unchanged but the higher frequency components are less evident.

Comparisons can also be made of the power spectra of the bending moment data and predictions. Since the

numerical solution of the equations of motion is based on a multipoint method that predicts based on previous steps, the calculation of power spectra is not valid at a frequency greater than 4p (approximately 2.8 Hz), even though this is less than the Nyquist frequency. The cut-off frequency can be extended by decreasing the calculation step size, however this was not considered necessary due to the small amount of energy at the higher frequencies. Plots of data and predicted power spectral density of the bending moment at both blade stations in Figures 4.9 and 4.10 show a slight increase in energy from the unsteady models at frequencies less than 1p that contribute to the higher predicted mean loads. Other than this small shift in the power spectral density, no other change in features is evident with the addition of unsteady aerodynamics. The expected decrease in energy at higher frequencies due to the shed wake effects is not a prominent feature. Results show no change when the convective model is used for the trailing wake instead of the unsteady momentum model.

Predictions were made of these same loads using different values of surface roughness length in the wind simulation program. Roughness lengths were chosen that span a reasonable range of values possible for the location of the Howden machine. The results shown in Figures 4.11 and 4.12 for the 1.5 m and 8.25 m blade stations, respectively, show only small differences in the power spectral density for the range on z_0 from 0.01 to 0.20. This shows that

there is little sensitivity as long as a reasonable guess is made for the roughness length.

4.3 Tower Motion

A degree of freedom for tower motion was included to examine the change in blade bending moment caused by tower dynamics and the aerodynamic coupling. Axial tower motion of the cantilevered tower was modeled as a simple mass-spring system as covered in Chapter 3. The value of mass is estimated to include the nacelle, rotor, and a fraction of the tower mass given by [6] as

$$m_{tip} = m_{nacelle} + 0.2427\ m_{tower} \qquad (4.3.1)$$

The equivalent mass and spring constants given in [1] are 19070 kg and 1.836×10^6 N/m, respectively. The addition of tower motion to the three-blade machine brings the total number of degrees of freedom to be analyzed to four.

The aerodynamic and structural coupling require that a set of eight simultaneous, coupled, nonlinear equations must be solved to determine acceleration and velocity of each blade and the tower. A problem arises in the solution caused by the fact that the nonlinear, second order equations of motion are highly sensitive to the initial conditions chosen, and convergence to the solution may not be possible for all choices. The addition of structural

damping was proposed to overcome this problem [1], but this causes a reduction in blade and tower deflections and a phase shift. The nonlinearity comes primarily from the aerodynamic terms since the dynamic expressions have been linearized. The linearized blade/tower dynamics excluding aerodynamic damping can be analyzed to estimate the eigenvalues and eigenvectors to predict system natural frequencies and mode shapes. The cyclic loads can be predicted by bin averaging the results of multiple revolutions if convergence to a single solution does not result from the choice of initial conditions.

The eigenvalues are found from the equation

$$[m]\{q\} + [k]\{q\} = \{0\} \qquad (4.3.1)$$

where the mass matrix [m] and the stiffness matrix [k] are defined by equation 3.5.14. For the Howden machine, these become

$$[m] = \begin{bmatrix} 262.9 & 0.0 & 0.0 & 396.0 \\ 0.0 & 262.9 & 0.0 & 396.0 \\ 0.0 & 0.0 & 262.9 & 396.0 \\ 396.0 & 396.0 & 396.0 & 22478.0 \end{bmatrix} \quad \text{kg}$$

$$[k] = \begin{bmatrix} 27360.9 & 0.0 & 0.0 & 0.0 \\ 0.0 & 27360.9 & 0.0 & 0.0 \\ 0.0 & 0.0 & 27360.0 & 0.0 \\ 0.0 & 0.0 & 0.0 & 1.836E6 \end{bmatrix} \quad \text{N/m}$$

The eigenvalues and eigenvectors were extracted using an iterative procedure giving the frequencies and mode shapes presented in Table 4.2. The lowest frequency, 1.33 Hz, is

found when all three blades and the tower move in-phase. This frequency is nearest the 2p harmonic and as a result is highly excited as seen in the bending moment power spectral density as seen previously in Figures 4.9 and 4.10. Two identical frequencies of 1.62 Hz correspond to the blade natural frequency with a rigid tower including blade stiffening from rotation. The highest frequency of 1.83 Hz corresponds to the mode shape where blades and tower are 180 degrees out of phase. The 1.62 Hz and 1.83 Hz fall between the 2p (1.4 Hz) and 3p (2.1 Hz) harmonics and show no definable response in the bending moment spectrum. The resonant frequency of the cantilever tower with the suspended nacelle mass is approximately 1.44 Hz. There is very little excitation of the tower since it falls well below the 3p excitation from the combined thrust of the three blades.

Figure 4.14 shows a comparison with data for cyclic steady state bending moment with steady wind at the 8.25 m blade station for cases with and without tower motion. There was no difference in the mean loads, and very little difference in the cyclic results caused by tower motion. Comparison of the bending moment power spectral density for these cases was not done since the turbulent wind simulation code does not generate a spectrum for more than one blade. The four degree of freedom model does provide valuable information on the tuning of the one degree of freedom to the correct natural frequency of the blade/tower axial

motion. This is especially critical in the case of the Howden machine where the blade natural frequency is so near the multiple of the rotational frequency.

Table 4.1 Mean Loads Comparison for Data Set 12-7 at a Mean Wind Speed of 10.9 m/s

	TORQUE (N-m)	THRUST (N)	BENDING MOMENT @ 1.5 M (N-m)	BENDING MOMENT @ 8.25 M (N-m)
DATA AVERAGE	52105	21700	61100	9050
STEADY WIND STEADY AERO	38800	24800	43200	7030
STEADY WIND UNSTEADY AERO	38600	24800	43200	7020
TURBULENT WIND STEADY AERO	38700	24400	42500	7000
TURBULENT WIND UNSTEADY AERO	59400	36200	63500	10400

Table 4.2 Frequencies and Mode Shapes for Four Degree-of Freedom Model

FREQUENCY	MODE SHAPE
1.33 Hz	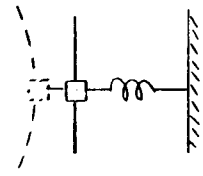 {q}={1,1,1,0.17}
1.62 Hz	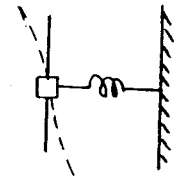 {q}={1,1,-2,0}
1.62 Hz	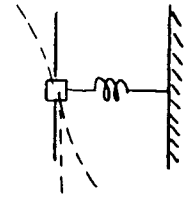 {q}={1,-1,0,0}
1.83 Hz	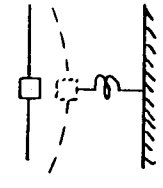 {q}={1,1,1,-0.2}

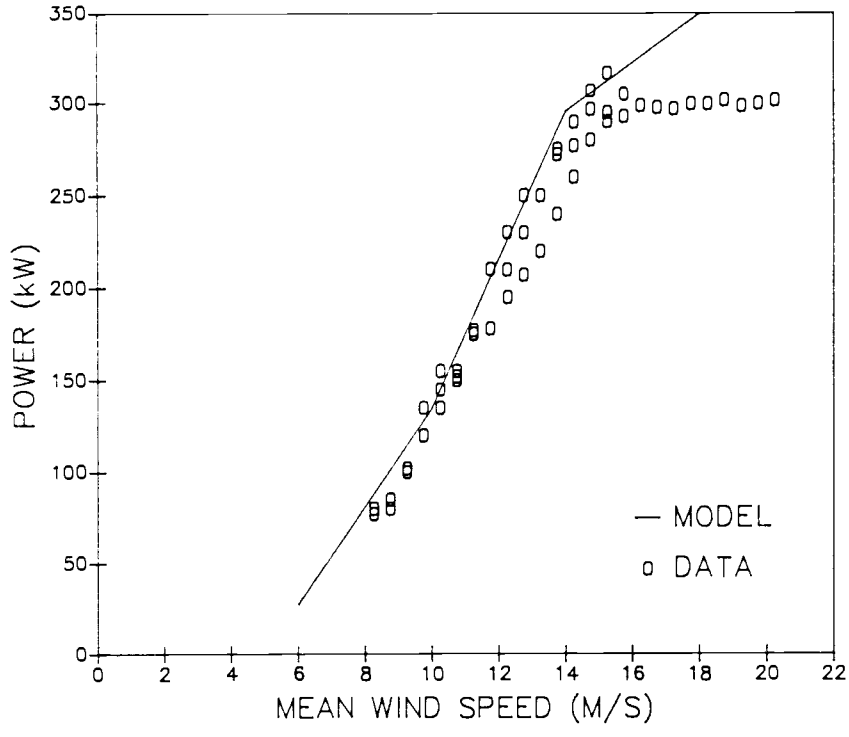

Figure 4.1 Mean Power Curve

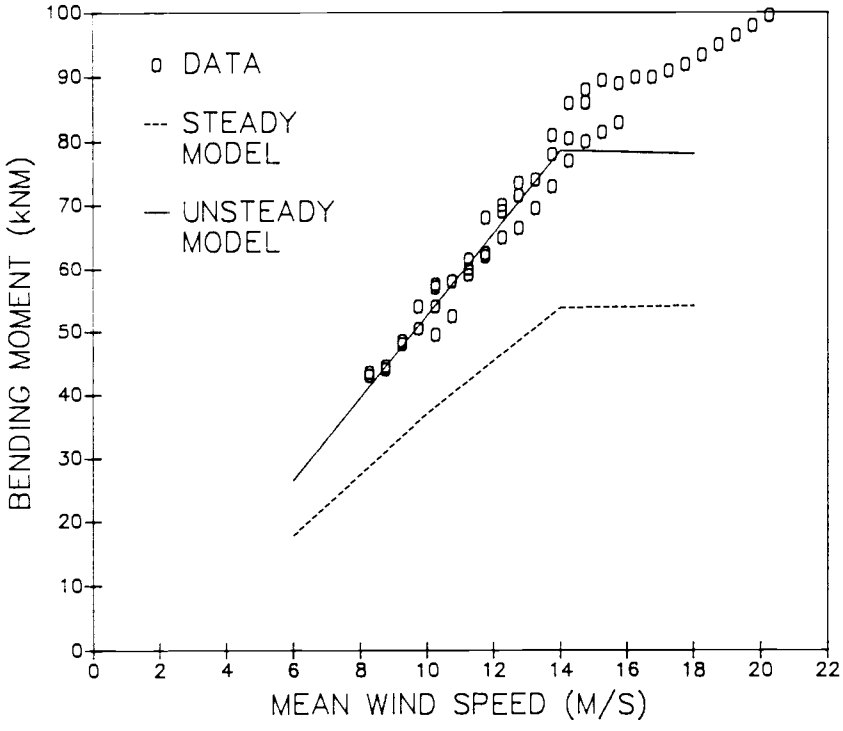

Figure 4.2 Mean Flap Bending Moment at 1.5 m

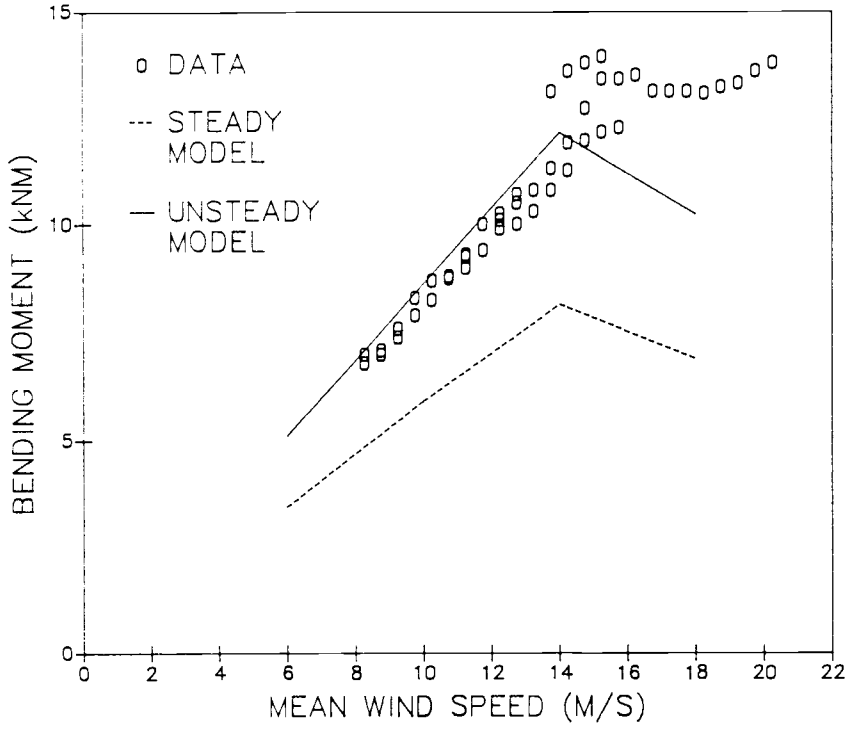

Figure 4.3 Mean Flap Bending Moment at 8.25 m

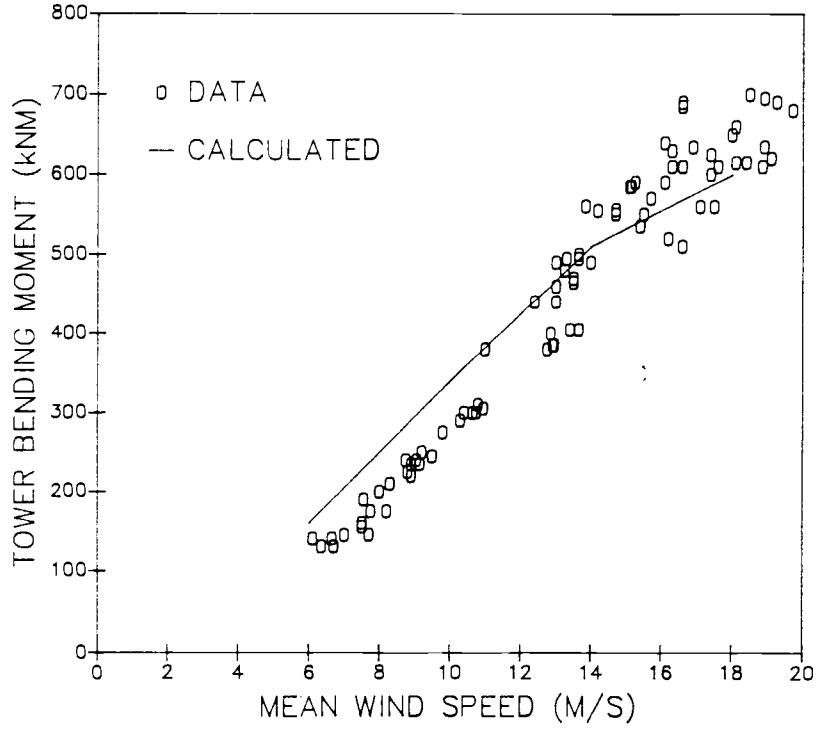

Figure 4.4 Comparison of Measured and Calculated Mean Tower Bending Moment

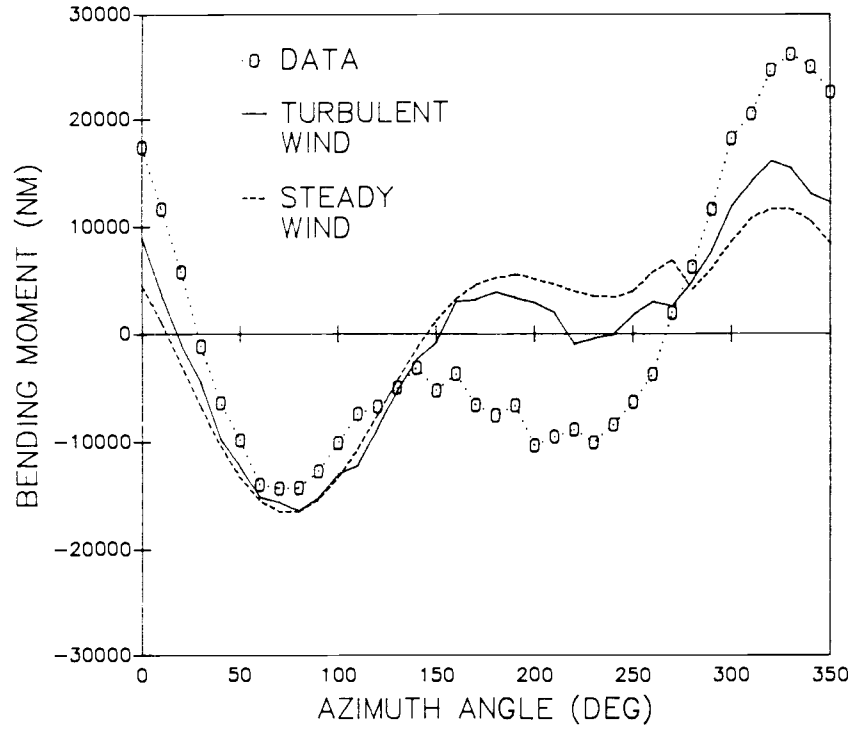

Figure 4.5 Cyclic Bending Moment at 1.5 m with Steady State Aerodynamics

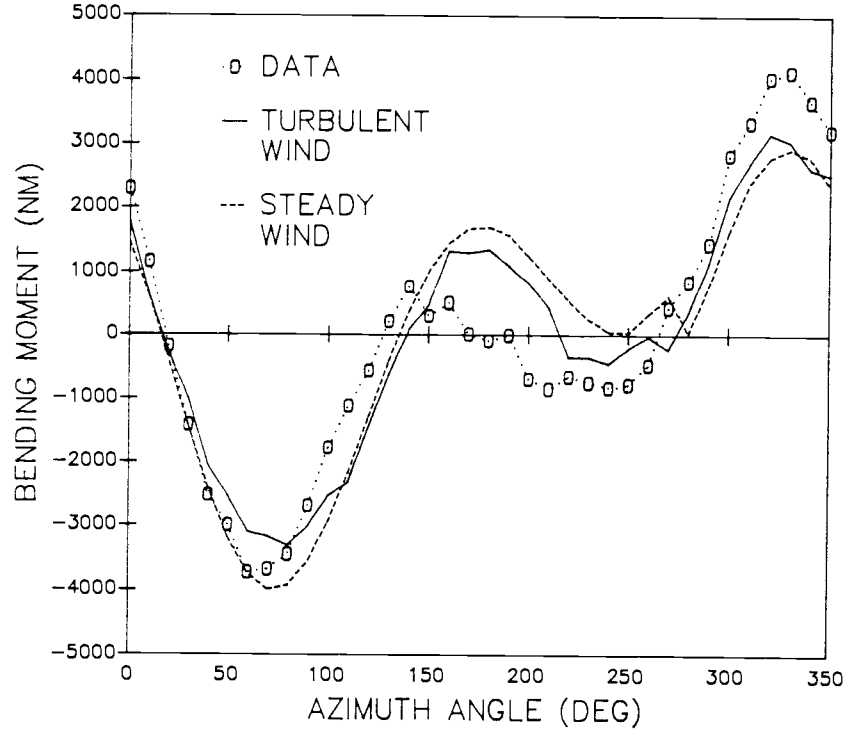

Figure 4.6 Cyclic Bending Moment at 8.25 m with Steady State Aerodynamics

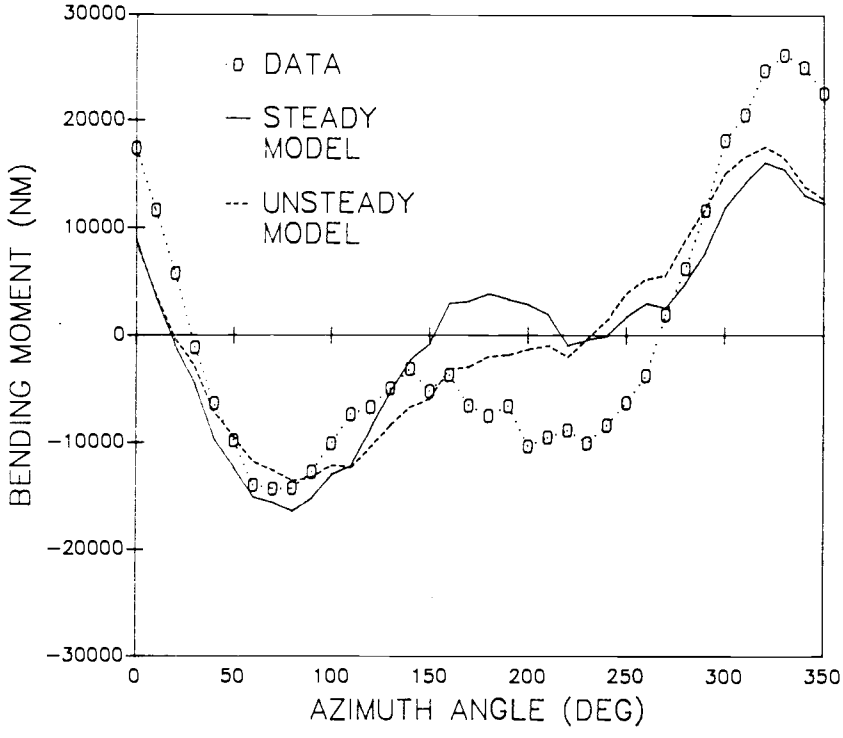

Figure 4.7 Cyclic Bending Moment at 1.5 m with Turbulent Wind

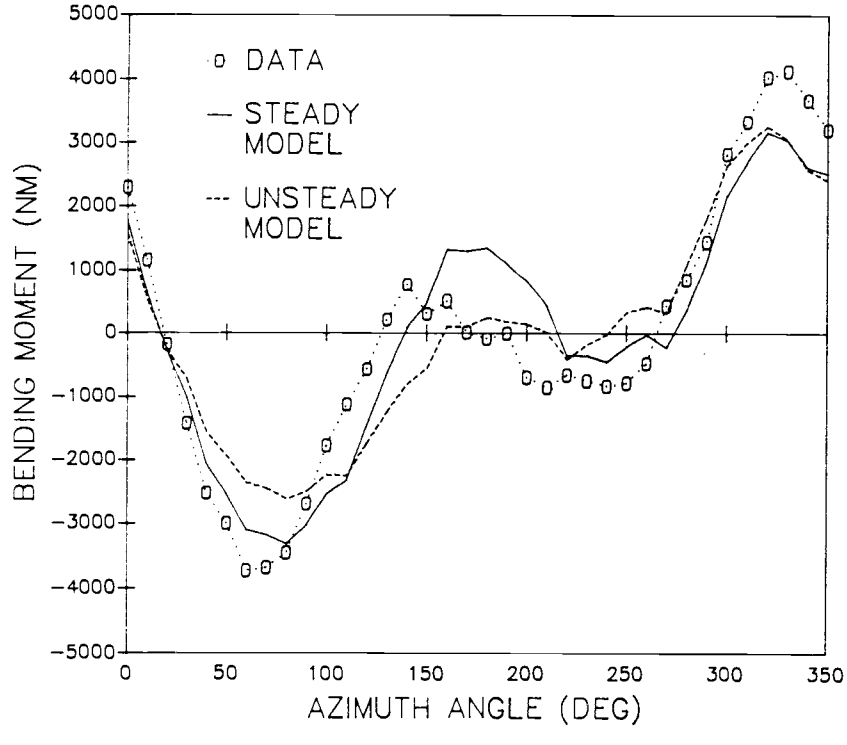

Figure 4.8 Cyclic Bending Moment at 8.25 m with Turbulent Wind

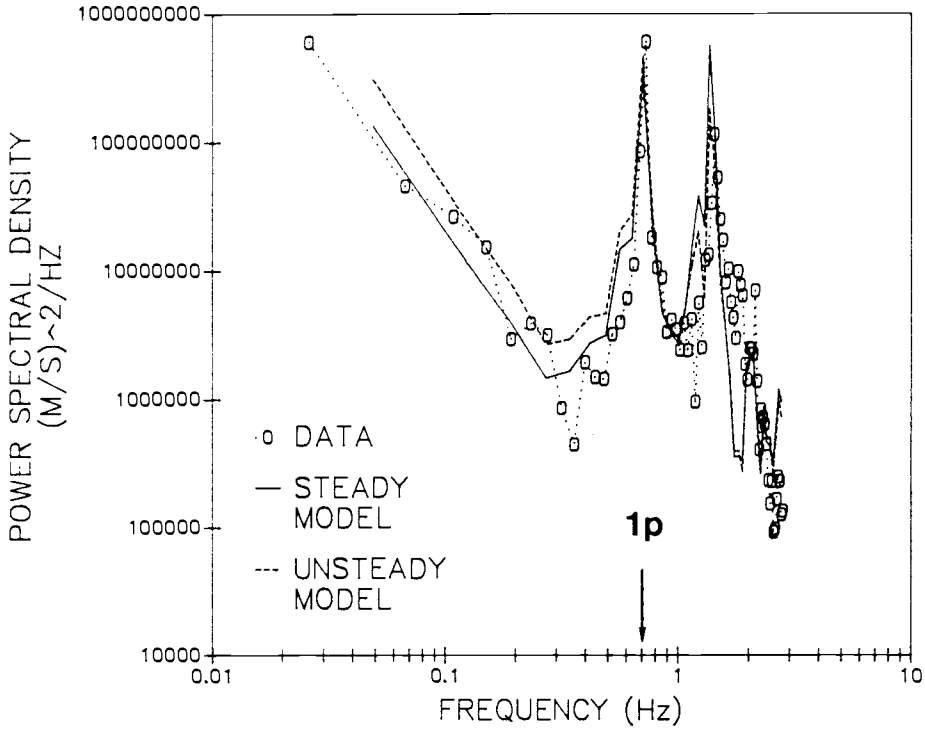

Figure 4.9 Bending Moment Power Spectral Density at 1.5 m

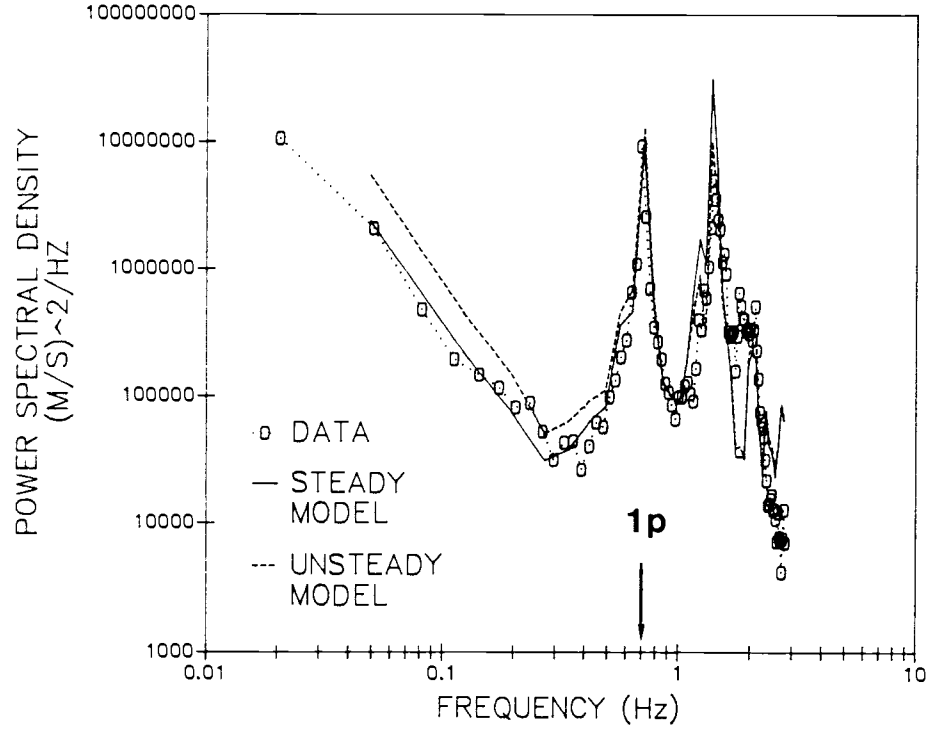

Figure 4.10 Bending Moment Power Spectral Density at 8.25 m

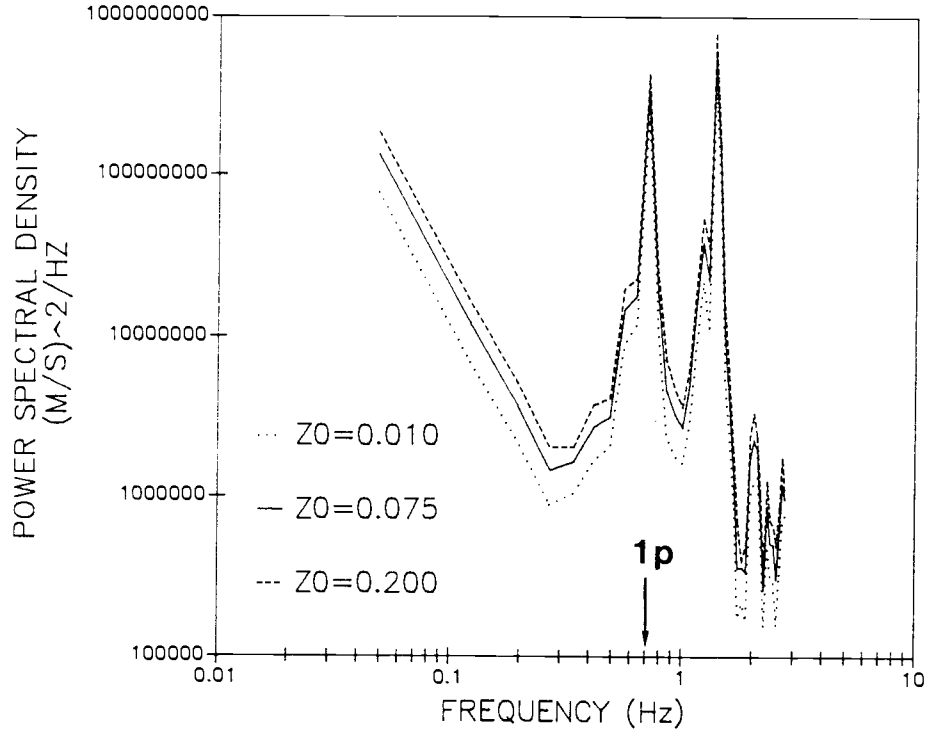

Figure 4.11 Effect of Surface Roughness Length on Moment Power Spectral Density at 1.5 m

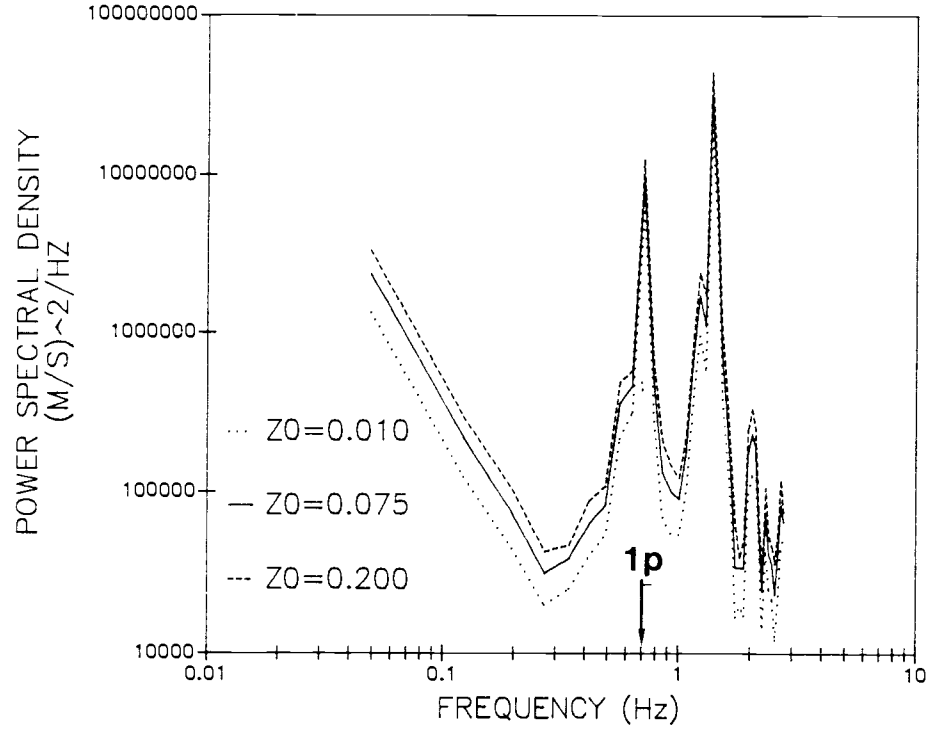

Figure 4.12 Effect of Surface Roughness Length on Moment Power Spectral Density at 8.25 m

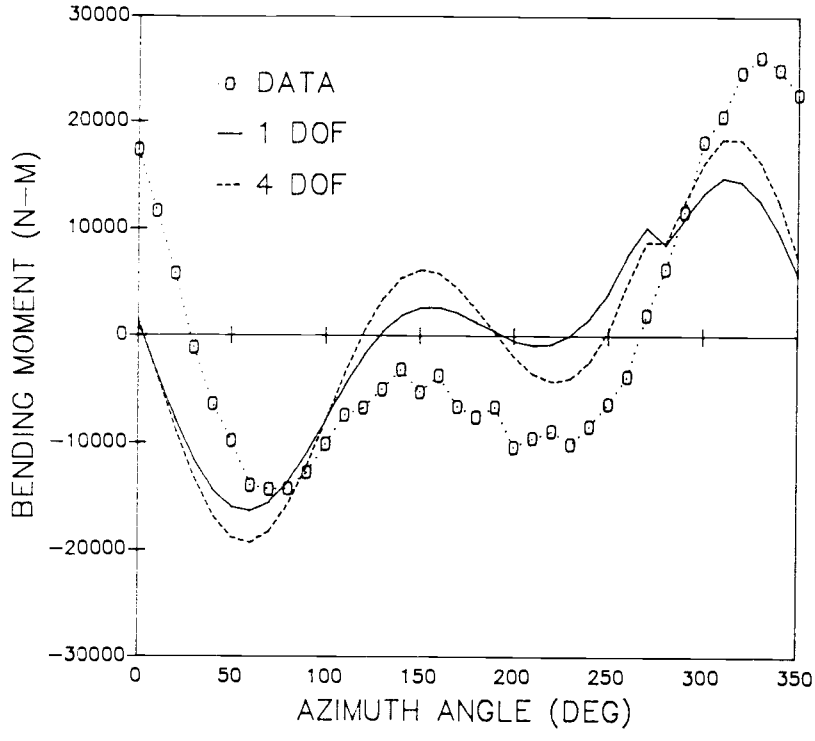

Figure 4.13 Effect of Tower Motion on Cyclic Bending Moment at 1.5 m

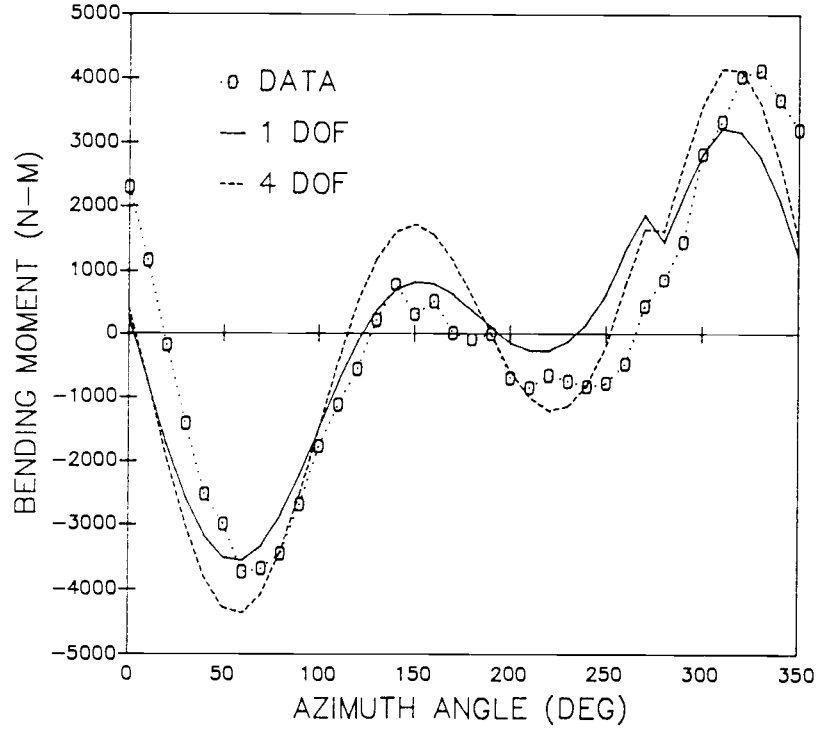

Figure 4.14 Effect of Tower Motion on Cyclic Bending Moment at 8.25 m

4.4 References

1. Wehrey, M., Redmond, I., Anderson, C. and Jamison, P., "Dynamic Response of a 330-kW Horizontal Axis Wind Turbine," SERI Report SERI/STR-217-3203, February 1988.

2. Madsen, P.H., Hock, S.M., and Hausfeld, T.E., "Turbulence Loads on the Howden 26-m Diameter Wind Turbine," SERI Report SERI/TP-217-3269, November 1987.

3. Hock, S.M., Hausfeld, T.E., Hampton, G., and Thresher, R.W., "Preliminary Results form the Dynamic Response Testing of the Howden 330-kW HAWT," SERI Report SERI/TP-3243.

4. Wright, A.D. and Thresher, R.W., "Accurate Rotor Loads Prediction Using the FLAP Dynamics Code," SERI Report SERI/TP-3223.

5. Madsen, P.H., "DAP - 1, A Data Analysis Package for Spectral Analysis, Version 1.2," SERI Report 217/DRAFT/WRB1075, November 1987.

6. Tse, F.S., Morse, I.E., and Hinkle, R.T., Mechanical Vibrations, 2nd Edition, Allyn & Bacon Inc., 1978.

CHAPTER 5

SUMMARY AND CONCLUSIONS

The objective of this effort was to develop models of unsteady aerodynamics related to the shed wake and the trailing wake and determine the resulting blade loads for a wind turbine experiencing variable incident wind. Judgment on the value of the addition of unsteady aerodynamics can then be based on the improvement in the predictive ability for mean loads, cyclic loads, or the power spectral density of loads, depending on the design criteria. Additionally, the sensitivity of the loads prediction to changes in design parameters such as blade and tower resonant frequency, airfoil design, mean wind, or wind turbulence intensity can be investigated. In this study, no attempt was made to conduct a parametric analysis or extensively characterize the effects of unsteady aerodynamics over a broad range of operating conditions. Rather, the emphasis has been to verify the models by comparison to a few selected data sets where significant documentation exists. One disadvantage of the modeling techniques for conducting parametric studies is the formulation of the equations for time domain solution. Linearized models that yield analytic frequency domain solutions are better suited to that type of study at the sacrifice of the information contained in the non-linear effects.

5.1 Aerodynamic Modeling Results

The shed wake effects that cause a lag in airfoil circulation were modeled as a first order effect that can be characterized by a single time constant. The model, developed to treat the case of an airfoil undergoing translatory oscillations, includes the circulatory lift terms that are wake dependent and the non-circulatory terms that are motion dependent. The single-parameter model was compared to both an analytic solution of the problem and a vortex method solution for a prescribed sinusoidal input and showed very good agreement over much of the frequency range. However, this approximate method is suitable for time domain solution for any arbitrary airfoil displacement and wind velocity, and does not require the computer time of methods that do extensive wake calculations. The disadvantages of the single-parameter method lie both in the accuracy of the approximation to the true solution for the translating airfoil, and the error due to the rotational nature of the wake. The approximation does not include any correction for the shed vortex not being parallel, the displacement of the wake downstream, or the interference with the vortex shed by the leading blades. For certain ranges of values of tip speed ratio, these effects are certainly second order, but this does limit the universal applicability of this approach. Some empirical tailoring of the time constant to

reflect these conditions might extend the usefulness of this method, but that would defeat the purpose of a predictive program.

The trailing wake effects that cause a lag in rotor induction were modeled with two different first order models. The convective model is developed from a theory proposed by Montgomerie to obtain the lag time constant directly from a simplified wake model. Simplifying the trailing wake as a series of rings rather than a helix and ignoring wake expansion, the change in centerline axial induction after a step change in wind is used to estimate the induction time constant from the approximately exponential growth in induced velocity. The second approach developed an axial unsteady momentum theory that generates a first order equation with an imbedded time constant that depends mainly on the apparent mass of the air that is accelerated or decelerated through the rotor disk after a step change in velocity. Ignoring the second order effects of wake expansion and rotational components of induced velocity, a comparison of these methods at conditions representative of wind turbine operating conditions gave time constants that differed by fifty percent, with the convective method giving a longer time constant for all cases. Comparison of these results to data and the analysis of others give contradictory indications that the predicted time constant is too short in one case and too long in another. It is obvious that a more complete theory is

needed for the lag of induction caused by the trailing wake. One consolation is that both time constant predicted by the simplified theories are bounded by values obtained from other sources, and neither method resorts to any empiricism.

5.2 Loads Results

The results of the comparisons for two selected wind turbines show that the addition of unsteady aerodynamics improves the prediction of the level of mean loads for turbulent wind conditions. This is due to the strong influence of the long time constant for the trailing wake. The cyclic loads predictions show a smoothing of the cyclic variation due to the shorter shed wake time constant, but this prediction is not born out by the data. The predictions for bending moment power spectral density reflects an increase in load at the lower frequencies less than one per period and a very slight decrease at higher frequencies between 1p and 3p due to unsteady effects. Overall, the shed wake effects do not significantly effect the loads.

The inclusion of tower axial motion has a small effect on the cyclic loads and no noticeable effect on the mean loads. In the case of the Howden machine, the tower resonant frequency of 1.44.Hz lies well below the excitation frequency of 3p and the resulting motion is small and there

is very little effect of the aeroelastic coupling. Since the results of the prediction are very sensitive to the resonant frequency of the coupled blade/tower motion, the value of adding tower motion and performing calculations for four degrees of freedom is to obtain an estimate of the mode shapes and frequencies.

5.3 Code Predictions

The ability of the techniques described to predict loads with a fair amount of accuracy has been demonstrated. The only adjustable constants deal with the multipliers of blade mass and stiffness distribution, and these are used to "tune" the blade/tower resonant frequency. This could either be done using data on the measured frequency of the rotating blade or the predictions of eigenvalues form the blade/tower model. The predictive ability of this code, or any code for that matter, is also influenced by how well defined the design parameters are and how well the wind conditions, including turbulence levels, are known. This code has shown, for example, that the results are highly sensitive to small changes in blade parameters but very insensitive to small changes in surface roughness length. The inclusion of trailing wake unsteady effects is necessary to obtain good predictions of mean loads in a turbulent

wind, but the shed wake unsteady effects show little or no improvement in loads prediction.

5.4 Areas for Future Work

Some areas where future work is necessary are evident from the work performed here. These are

a) A better theory is needed to predict the time constant for the trailing wake. Neither method developed here was in full agreement with the limited amount of data. Also, a more complete theory including rotational effects may be required to determine shed wake effects.

b) A model is needed to analyze wind turbines of more complicated geometry and to include teetering rotors, edgewise blade flexing, variable speed rotors, pitch control algorithms, and a yaw degree of freedom, for example.

c) A turbulence code for a multiblade rotor is required to analyze the effects of turbulence when additional rotor degrees of freedom are added.

d) Additional data is required to fully evaluate the shed and trailing time constants under a larger range of operating conditions.

BIBLIOGRAPHY

Batchellor, G.K., An Introduction to Fluid Dynamics, Cambridge University Press, 1967.

Bramwell, Helicopter Dynamics, Edward Arnold Ltd., London, 1976.

Carpenter, P.J. and Fridovitch, B., "Effect of Rapid Pitch Increase on the Thrust and Induced Velocity Response of a Full Scale Helicopter," NACA TN 3044, 1953.

Connell, J.R., "The Spectrum of Wind Speed Fluctuations by a Rotating Blade of a Wind Energy Conversion System," Solar Energy, Vol. 29, No. 5, pp. 363-375, 1982.

Counihan, J., "Adiabatic Atmospheric Boundary Layers: A Review and Analysis of Data from the Period 1880-1972," Atmospheric Environment, Vol. 9, pp. 871-915, 1975.

Dinyavari, M.A.H. and Friedmann, P.P., "Application of Time-Domain Aerodynamics to Rotary Wing Aeroelasticity," AIAA J., Vol. 24, No. 9, 1986.

Dinyavari, M.A.H. and Friedmann, P.P., "Time Domain Unsteady Incompressible Cascade Airfoil Theory for Helicopter Rotors in Hover," AIAA J., Vol. 27, No. 3, 1989.

Djojodihardjo, R.H. and Widnall, S.E., "A Numerical Method for Calculation of Nonlinear Unsteady Lifting Potential Flow Problems," AIAA J., Vol. 7, No. 10, 1969.

Frost, W., Long, B.H., and Turner, R.E., "Engineering Handbook on the Atmospheric Environmental Guidelines for Use in Wind Turbine Generator Development," NASA Tech. Paper 1359, 1978.

Froude, R.E., Transactions, Institute of Naval Architects, Vol. 30, p. 390, 1889.

Gerald, C.F. and Wheatley, P.O., Applied Numerical Analysis, Addison-Wesley, 1984.

Glauret, H., "The Analysis of Experimental Results in Windmill Brake and Vortex Ring States of an Airscrew," Reports and Memoranda, No. 1026, 1926.

Glauret, H., "On Contraction of the Slipstream of an Airscrew," ARC Reports and Memoranda, No. 1067, 1926.

Gohard, J.D., "Free Wake Analysis of Wind Turbine Aerodynamics," MIT Aeroelastic and Structures Lab, Cambridge, MA, TR 184-14, September 1978.

Goldstein, S., "On the Vortex Theory of Screw Propellors," Proc. Royal Soc. A123, p. 440, 1929.

Graber, A. and Rosen, A., "Velocities Induced by Semi-Infinite Helical Vortex Filaments," J. Aircraft, Vol. 24, No. 5, 1987.

Gray, R.B. and Brown, G.W., "A Vortex-Wake Analysis of a Single Bladed Hovering Rotor and a Comparison with Experimental Data," AGARD-CP-111, 1972.

Hess, J.L. and Smith, A.M.O., "Calculation of Potential Flow About Arbitrary Bodies," Prog. Aero. Sci., Vol. 8, 1967.

Hock, S.M., Hausfeld, T.E., Hampton, G., and Thresher, R.W., "Preliminary Results form the Dynamic Response Testing of the Howden 330-kW HAWT," SERI Report SERI/TP-3243, October 1987.

Johnson, W., "Recent Developments in Rotary Wing Aerodynamic Theory," AIAA J., Vol. 24, No. 8, 1986.

Johnson, W., Helicopter Theory, Princeton University Press, 1983.

Kane, T.R. and Levison, D.A., Dynamics: Theory and Applications, McGraw-Hill, Inc., 1985.

Kottapalli, S.B.R. and Friedmann, P.P., "Aeroelastic Stability and Response of Horizontal Axis Wind Turbine Blades," AIAA J., Vol. 17, No. 12, 1979.

Kussner, H.G., "Zusammenfassender Bericht uber den instationaren Auftrieb von Flugeln," Luftfahrtforschung, Bd. 13, Nr. 12, pp. 410-424, 1936.

Loewy, R.G., "A Two Dimensional Approximation to the Unsteady Aerodynamics of Rotary Wings," Jour. Aero. Sci., Vol. 24, No, 2, 1957.

Madsen, P.H., "DAP - 1, A Data Analysis Package for Spectral Analysis, Version 1.2," SERI Report 217/DRAFT/WRB1075, November 1987.

Madsen, P.H., Hock, S.M., and Hausfeld, T.E., "Turbulence Loads on the Howden 26-m Diameter Wind Turbine," SERI Report SERI/TP-217-3269, November 1987.

McGhee, R.J. and Beasley, W.D., "Effects of Thickness on the Aerodynamic Characteristics of an Initial Low-Speed Family of Airfoils for General Aviation Applications," NASA-TM-X-72843, 1976.

Miller, R.H., "Methods for Rotor Aerodynamic and Dynamic Analysis," Prog. Aero. Sci., Vol. 22, 1985.

Montgomerie, B., "Unsteady Aerodynamics Applied to Horizontal Axis Wind Turbine Disk," National Aeronautical Laboratory, Sweden, FFA Memo, November 1984.

Ormiston, R.A. and Peters, D.A., "Hingeless Helicopter Rotor Response with Non-Uniform Inflow and Elastic Bending," J. Aircraft, Vol. 9, No. 10, 1972.

Oye, S., "Unsteady Wake Effects Caused by Pitch-Angle Changes," Aerodynamics of Wind Turbines Symposium, Technical Univ. of Denmark, October 1986.

Peters, D.A., "Hingeless Rotor Frequency Response with Unsteady Inflow," AHS/NASA-Ames Specialists' Meeting on Rotorcraft Dynamics, February 13-15, 1974.

Pitt, D.M. and Peters, D.A., "Theoretical Prediction of Dynamic Inflow Derivatives," Vertica, Vol. 5, 1981.

Piziali, R.A., "Method for Solution of the Aeroelastic Response Problem for Rotating Wings," J. Sound Vib., Vol. 4, No. 3, 1966.

Powell, D.C. and Connell, J.R., "A Model for Simulating Rotational Data for Wind Turbine Applications," PNL-5857, April 1986.

Prandtl, L., Gottinger Nachr., p. 193, 1919.

Preuss, R.D., Suciu, E.O., and Morino, L., "Unsteady Potential Aerodynamics of Rotors with Applications to Horizontal Axis Windmills," AIAA J., Vol. 18, No. 4, 1980.

Rankine, W.J.M., Transactions, Institute of Naval Architects, Vol. 6, p. 13, 1865.

Satran, D. and Snyder, M.H., "Two-Dimensional Tests of GA(W)-1 and GA(W)-2 Airfoils at Angles-of-Attack from 0 to 360 Degrees," WER-1, Wind Energy Laboratory, Wichita, Kansas, January 1977.

Summa, J.M., "Potential Flow about Three Dimensional Streamlined Lifting Configurations with Applications to Wings and Rotors," AFOSR-TR-74-1914, 1974.

Theodorsen, T., "General Theory of Aerodynamic Instability and the Mechanism of Flutter," NACA TR 496, 1935.

Tse, F.S., Morse, I.E., and Hinkle, R.T., Mechanical Vibrations, 2nd Edition, Allyn & Bacon Inc., 1978.

Van Holten, T., "Computation of Aerodynamic Loads on Helicopter Rotor Blades in Forward Flight Using the Method of Acceleration Potential," 9th Congress Inter. Counc. Aero. Sci., Aug. 25-30, 1974.

Venkatesan, C. and Friedmann, P.P., "New Approach to Finite-State Modeling of Unsteady Aerodynamics," AIAA J., Vol. 24, No. 12, 1986.

von Karman, T. and Sears, W., "Airfoil Theory for Non-Uniform Motion," J. Aero. Sci., Vol. 5, No. 10, 1978.

Wagner, H., "Uber die Entstehung des dynamischen Auftriebes von Tragflugeln," Zeitschrift fur angewandte Mathematik und Mechanik, Vol. 5, No. 1, 1925.

Warmbrodt, W. and Friedmann, P.P., "Coupled Rotor/Tower Aeroelastic Analysis of Large Horizontal Axis Wind Turbines," AIAA J., Vol. 18, No. 9, 1980.

Wehrey, M., Redmond, I., Anderson, C. and Jamison, P., "Dynamic Response of a 330-kW Horizontal Axis Wind Turbine," SERI Report SERI/STR-217-3203, February 1988.

Wilson, R.E. et. al., "Aerodynamic Loads on a Darrieus Rotor Blade," J. Fluids Eng., Vol. 105, March 1983.

Wilson, R.E. and Walker, S.N., "Performance Analysis of Horizontal Axis Wind Turbines," NASA-NAG-3-278, September 1984.

Wilson, R.E., Walker, S.N., Weber, T.L. and Hartin, J.R., "A Comparison of Mean Loads and Performance Predictions with Experimental Measurements for Horizontal Axis Wind Turbines," Eighth ASME Wind Energy Symposium, Houston, Texas, Jan. 22-29, 1989.

Wright, A.D. and Thresher, R.W., "Accurate Rotor Loads Prediction Using the FLAP Dynamics Code," SERI Report SERI/TP-3223, October 1987.

APPENDIX

APPENDIX A

HOWDEN WIND TURBINE DESCRIPTION

The wind turbine used as the basis of these experiments was a Howden three-blade, upwind, horizontal-axis machine with a rigid hub and wood/epoxy blades. The tests were conducted in Palm Springs, CA as a joint effort between the Solar Energy Research Institute and James Howden and Co. as part of the Cooperative Field Test Program of the Department of Energy.

The HWP 330/26 has a rated power of 330 kW at a hub-height wind speed of 14.5 m/s (32 mph). Figure A.1 shows the major dimensions of the installation. It was designed to operate at a cut-in wind speed of 6 m/s and a cut-out wind speed of 28 m/s. The rotor diameter is 26 m and it rotates at a constant speed of 42 RPM. The blades are tapered and twisted, with a maximum chord of 1.47 m and a maximum twist angle of 16 degrees at a radius of 0.64 m. The chord and twist decrease linearly to 0.79 m and 0 degrees, respectively, at the tip. The blade airfoil is a GA(W)-1, 17% thick. The lift and drag coefficients used in the program are a curve fit of airfoil data from [1,2]. The curve fit of the coefficients is plotted in Figure A.2. Power is controlled above the rated speed using a variable pitch. The tip pitch is held constant at 0 degrees pitch for wind speeds up to rated speed of 14.5 m/s. Above rated wind speed, the experimental data gives a linear increase in

tip angle up to approximately 11 degrees at a wind speed of 18 m/s. A summary of machine dimensions is given in Table A.1 and a summary of blade dimensions is given in Table A.2. The mass and stiffness distributions used as input to the model are given in Table A.3.

Table A.1 Machine Dimensions

Rotor Axis Centerline Height	= 24.1 m
Rotor Diameter	= 26.0 m
Rotor Preconing Angle	= 0.0 deg.
Tower Diameter	= 1.8 m
Distance from Yaw Axis to Rotor Plane	= 3.5 m

Table A.2 Blade Dimensions

Radius (m)	Chord (m)	Pitch (deg)	Note
0.40	0.64	16.0	Blade Root
3.00	1.47	16.0	Blade "knee"
11.00	0.93	3.2	Tip Joint
13.00	0.79	0.0	Blade Tip

Table A.3 Mass and Stiffness Distribution

Radius (m)	Mass/Length (kg/m)	Stiffness (EI) (N/m)
0.40	150.6	4.54×10^7
0.7	150.6	4.54×10^7
1.5	103.6	2.96×10^7
2.5	59.7	1.50×10^7
3.5	63.2	7.75×10^6
4.5	60.2	8.30×10^6
5.5	57.4	6.36×10^6
6.5	54.5	2.82×10^6
7.5	51.7	2.21×10^6
8.5	36.5	1.66×10^6
9.5	36.5	1.38×10^6
10.5	34.6	1.38×10^6
11.15	89.6	2.76×10^6
11.45	112.0	7.20×10^6
11.79	83.1	6.92×10^6
12.57	52.9	4.15×10^6
13.0	52.9	4.15×10^6

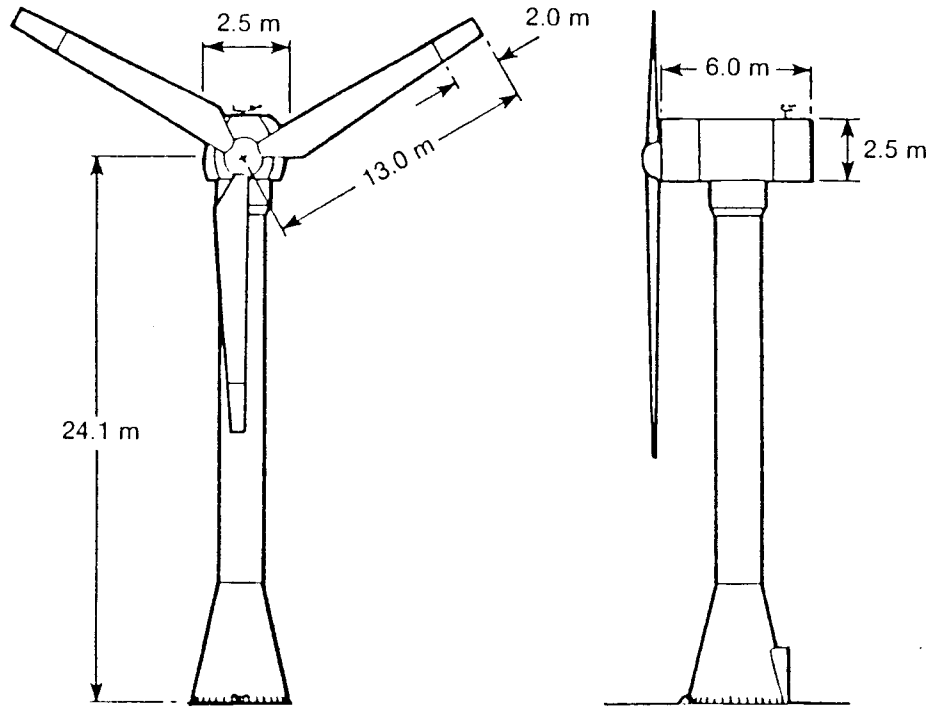

Figure A.1 Principal Dimensions

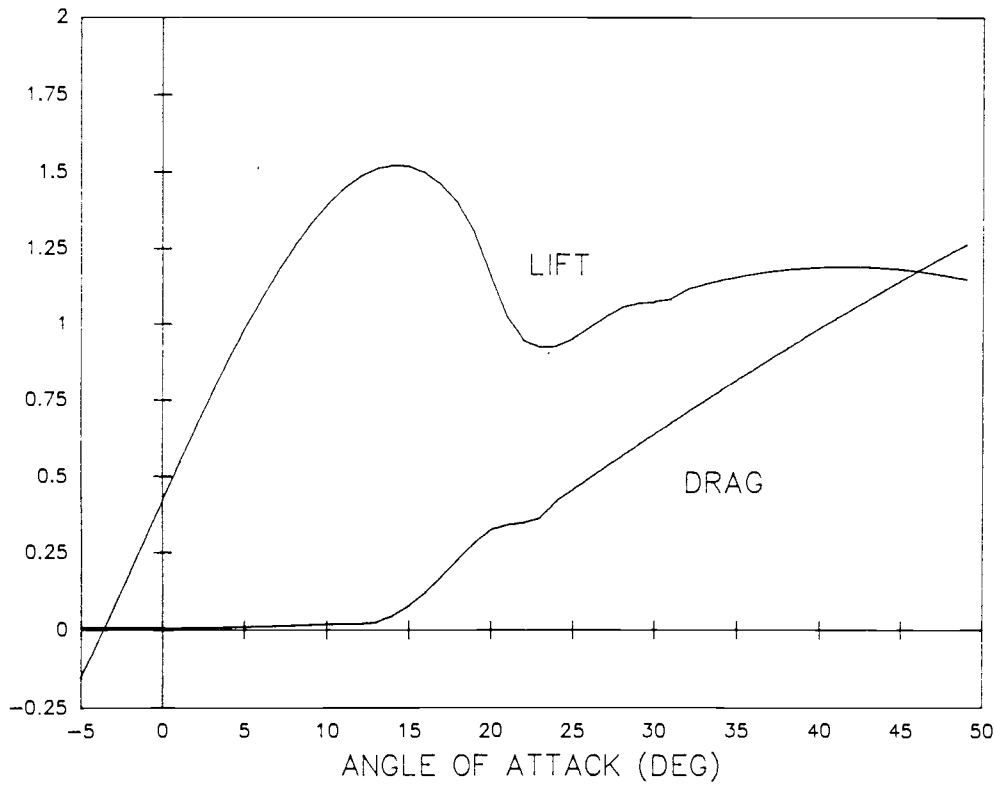

Figure A.2. Lift and Drag Coefficients for the GA(W)-1 Airfoil

A.1 References

1. McGhee, R.J. and Beasley, W.D., "Effects of Thickness on the Aerodynamic Characteristics of an Initial Low-Speed Family of Airfoils for General Aviation Applications," NASA-TM-X-72843, 1976.

2. Satran, D. and Snyder, M.H., "Two-Dimensional Tests of GA(W)-1 and GA(W)-2 Airfoils at Angles-of-Attack from 0 to 360 Degrees," WER-1, Wind Energy Laboratory, Wichita, Kansas, January 1977.